

# Computational analysis of the effect of hydrogen peroxide addition on premixed laminar hydrogen/air flames

Efstathios-Al. Tingas

*School of Engineering and the Built Environment, Edinburgh Napier University, Edinburgh EH10 5DT, United Kingdom*

---

## Abstract

In the current work, the effect of  $\text{H}_2\text{O}_2$  addition on the flame structure, laminar flame speed and NOx emissions is investigated in the context of 1D laminar premixed  $\text{H}_2$ /air flames at  $T_u=300$  and  $600$  K,  $p=1$  and  $30$  atm,  $\phi=0.5$ . Mathematical tools from the computational singular perturbation approach are used in order to identify the key chemical and transport mechanisms.

The  $\text{H}_2\text{O}_2$  addition causes a significant increase to the laminar flame speed ( $s_L$ ), heat release ( $Q$ ) and NOx emissions. Indicatively, 10%  $\text{H}_2\text{O}_2$  addition (per fuel volume) at  $T_u=300$  K,  $p=1$  atm results in 72% increase of  $s_L$ , 100% increase of  $Q$ , and 140% increase of the mass fraction of NO. Depending the conditions the flame structure is altered through the chain carrying reaction 10f ( $\text{H}_2\text{O}_2 + \text{H} \rightarrow \text{H}_2\text{O} + \text{OH}$ ) or the chain branching 9f ( $\text{H}_2\text{O}_2 (+\text{M}) \rightarrow 2\text{OH} (+\text{M})$ ); the first is favored at low temperatures/pressures while the latter is favored at sufficiently high temperatures/pressures. Both reactions boost the radical pool generation, therefore contributing to the broadening of the reaction zone. The reaction with the largest contribution to  $Q$  that is mostly affected (decreased) by the addition of  $\text{H}_2\text{O}_2$  is reaction 21 ( $\text{H} + \text{O}_2 (+\text{M}) \leftrightarrow \text{HO}_2 (+\text{M})$ ). Moreover, the  $\text{H}_2\text{O}_2$  addition enhances the stability of the flame. Finally, the increased production of NO is mainly associated with the increased temperature that is reached with the addition of  $\text{H}_2\text{O}_2$ .

*Keywords:* clean fuel, CSP, explosive mode, diesel engines, hydrogen, NOx

---

## 1. Introduction

The introduction of clean transportation modes, driven by the climate emergency, has become a priority for all modern economies. As a result, many nations have taken legislative measures to ensure, and in many cases to accelerate, the energy transition from fossil fuels to more environmentally friendly forms of energy. For instance, the UK government recently announced its commitment to end the sale of new petrol and diesel cars by 2030 accelerating its transition to net-zero emissions by 2050. To this direction, electric vehicles will play a key role exploiting the production of energy from renewable sources such as solar and wind energy. However, there are modes of transport where the electrification is still challenging, such as heavy-goods vehicles (HGVs) and ships. A common feature of these two types of transport is that currently

---

*Email address:* e.tingas@napier.ac.uk (Efstathios-Al. Tingas)

10 they are both powered predominantly by compression ignition (CI) engines.

Hydrogen is an energy carrier that has long been seen as an ideal candidate to replace fossil fuels in thermal engines [1–5]. Yet, its use in CI engines has mainly been attached to the dual fuel concept where a more reactive fuel, such as diesel, is employed to promote ignition [6]. To the best of the author’s knowledge, all the dual fuel concepts that have investigated the use of hydrogen in CI engines relied predominantly on  
15 carbon-based fuels [7], the only exceptions probably being that of ammonia [8] and ozone [9].

Recently, an alternative approach was proposed: that of a hydrogen-hydrogen peroxide blend ( $\text{H}_2\text{O}_2$ ) [10]. The use of hydrogen peroxide as an ignition promoter is not new. In fact, hydrogen peroxide has long been used in aerospace applications [11–14]. In conventional transport-related applications, hydrogen peroxide has been used with a large variety of fuels, such as natural gas [15, 16], diesel [17–23] and ammonia  
20 [24]. In the early work of Ref. [10] it was reported that a mere 10% (per fuel volume) addition of  $\text{H}_2\text{O}_2$  in  $\text{H}_2$ /air mixtures at homogeneous adiabatic and engine relevant conditions can lead to ignition delay times relevant to CI engines. The approach was also complemented by the addition of steam where it was showcased a spectacular decrease of  $\text{NO}_x$  emissions, while the ignition delay time was weakly affected and remained relevant to a CI engine operation. The work of Ref. [10] further examined the key chemical mechanisms related  
25 to the ignition delay time and  $\text{NO}_x$  emissions. The analysis of the chemical dynamics and the identification of the key chemical pathways was performed on the basis of mathematical tools from the computational singular perturbation (CSP) approach [25–28]. CSP is a mathematically rigorous algorithmic method of asymptotic analysis that has been used successfully in a large variety of different reacting flows set ups for the identification of the key chemical and transport mechanisms as well as for the characterisation of the  
30 reacting flow topology [29–37]. An excellent review on the potential of the CSP approach and its applications can be found in Ref. [38, 39]

The current study is a continuation of the earlier work reported in Ref. [10] and aims to investigate the effect of hydrogen peroxide addition on the flame structure, laminar flame speed and  $\text{NO}_x$  emissions, in the context of one-dimensional (1D) freely propagating premixed laminar flames. The reported findings  
35 and the drawn conclusions herein aim to explore further the potential and the limitations of the proposed technology. For that purpose algorithmic tools from the CSP approach will be employed to identify the key chemical mechanisms as well as their interaction with transport process that are important for the system’s dynamics.

The structure of the paper is as follows. Firstly, a brief overview of the CSP approach will be provided  
40 along with the mathematical tools as well as the computational set up. The simulations will be performed at three different sets of initial conditions to ensure an extended validity of the results and the drawn conclusions. The analysis of the results will follow, detailing first a reference case and discussing next the results from all the other cases.

## 2. Methods

45 The physical problem under investigation concerns an unstrained premixed freely propagating laminar flame. The PREMIX package [40] of the Chemkin Pro suite [41] is used for the simulations of the laminar flames. The reader is referred to the PREMIX manual for a detailed description of the employed numerical methods [40]. Since the physical problem is well documented in the literature [42], here only a brief description is provided.

The unstrained premixed freely propagating laminar flame problem can be mathematically described by the system of species and energy equations [40]:

$$\dot{m} \frac{dy_n}{dx} + \frac{d(\rho A y_n V_n)}{dx} - A \dot{\omega}_n W_n = 0 \quad (1)$$

$$c_p \dot{m} \frac{dT}{dx} - \frac{d}{dx} \left( \lambda A \frac{dT}{dx} \right) + A \sum_{n=1}^N \rho y_n V_n c_{p,k} \frac{dT}{dx} + A \sum_{n=1}^N \dot{\omega}_n h_n W_n = 0 \quad (2)$$

where  $x$  represents the spatial coordinates,  $T$  the temperature,  $y_n$  the mass fraction of species  $n$  ( $n=1,N$ ),  $\dot{\omega}$  the mass flow rate,  $\rho$  the mass density,  $W_n$  the molecular weight of species  $n$ ,  $\lambda$  the mixture's thermal conductivity,  $c_p$  the mixture's heat capacity at constant pressure,  $c_{p,k}$  the heat capacity at constant pressure of species  $n$ ,  $\dot{\omega}_n$  the molar rate of production of species  $n$  per unit volume,  $V_n$  the diffusion velocity of the  $n$ th species,  $A$  the cross-sectional area of the stream that contains the flame. Eqs. 1 and 2 are complemented by the continuity equation:

$$\dot{m} = \rho u A \quad (3)$$

as well as the equation of state:

$$\rho = \frac{pW}{RT} \quad (4)$$

50 where  $u$  is the velocity of the fluid mixture,  $W$  the mixture's mean molecular weight,  $p$  the pressure and  $R$  the universal gas constant. For the problem under study,  $\dot{m}$  is an eigenvalue and is determined as part of the solution. For this reason, the user must specify the temperature at one point, thereby fixing the location of the flame. For more details about the numerical solution methods used by PREMIX, the reader is referred to the manual [40].

55 The analysis of the pertinent chemical dynamics of the premixed flames discussed in the current study is performed using tools from the computational singular perturbation (CSP) approach [25]. For a detailed description of the method and the mathematical tools the reader is referred to Refs. [26, 38, 43, 44]. Here, only a brief description will be provided.

On the basis of solely the chemical source term (i.e., in the absence of transport), the system of species and temperature equations can be expressed in the form of Eq. 5:

$$\frac{dz}{dt} = \mathbf{g}(z) = \sum_{k=1}^{2K} \hat{\mathbf{S}}_k R^k, \quad (5)$$

where  $\mathbf{z}$  is a column vector with  $(N + 1)$  solution variables including  $N$  species mass fractions ( $\mathbf{y}$ ) and temperature ( $T$ ),  $\mathbf{g}(\mathbf{z})$  the chemical reaction source term, and  $\hat{\mathbf{S}}_k$  and  $R^k$  are the  $(N + 1)$ -dimensional generalized stoichiometric column vector and the reaction rate, respectively, of the  $k$ -th unidirectional reaction of a total of  $2K$  irreversible reactions [28, 44–46]. According to the CSP theory, Eq. (5) can be written in the form of Eq. 6:

$$\frac{d\mathbf{z}}{dt} = \sum_{i=1}^{N+1} \mathbf{a}_i h^i, \quad (6)$$

where  $\mathbf{a}_i$  is the  $(N + 1)$ -dimensional CSP basis column vector and  $h^i = \mathbf{b}^i \cdot \mathbf{g}(\mathbf{z})$  is the related amplitude, which is produced using the dual basis row vector  $\mathbf{b}^i$  ( $\mathbf{b}^i \cdot \mathbf{a}_j = \delta_j^i$ ) [25, 27, 47]. Interested in leading order accuracy, the CSP basis vectors  $\mathbf{a}_i$ ,  $\mathbf{b}^i$  can be approximated by the right ( $\boldsymbol{\alpha}_i$ ) and left ( $\boldsymbol{\beta}^i$ ), respectively, eigenvectors of the Jacobian  $\mathbf{J}$  of  $\mathbf{g}(\mathbf{z})$  [31, 34, 48–50]. Apart from an amplitude, each CSP mode is described by a timescale which is defined as the inverse norm of the associated eigenvalue, i.e.,  $\tau_i = |\lambda_i|^{-1}$ , where  $\lambda_i = \boldsymbol{\beta}^i \cdot \mathbf{J} \cdot \boldsymbol{\alpha}_i$  [51–53]. A CSP mode is characterised as explosive if the associated eigenvalue is positive and dissipative otherwise [50]. Explosive modes are relate to processes that tend to drive the system away from equilibrium. Such modes are typically met in igniting systems [36, 37, 54–57] and flames [58–64]. On the other hand, dissipative modes relate to processes which tend to drive the system towards equilibrium [65, 66].

The timescales of the modes are ordered from fast to slow and according to the criterion originally introduced in [29] and later revised in [67], the timescales (and the modes they associate with) can be classified as fast ( $\tau_1 < \dots < \tau_M$ ) and slow ( $\tau_{M+1} < \dots < \tau_{N+1}$ ) [68–70]. The fast timescales are responsible for the generation of the constraints in the phase space (i.e., the slow invariant manifold) on which the slow system evolves. Mathematically this means that Eq. 5 can be transformed in the system of:

$$h^m \approx 0 \quad (m = 1, M) \quad \frac{d\mathbf{z}}{dt} \approx \sum_{n=M+1}^{N+1} \mathbf{a}_n h^n. \quad (7)$$

In autoigniting systems described by Eq. 5, the system’s characteristic mode responsible for its slow evolution is usually of explosive nature since the associated timescale ( $\tau_{e,f}$ ) is among the fastest of the slow timescales ( $\tau_{e,f} \sim \mathcal{O}(\tau_{M+1})$ ) and its amplitude ( $h^{e,f}$ ) is dominant [71–74].

In the presence of transport (convection or diffusion or both), Eq. 5 can be written in the form of eq. 8:

$$\frac{d\mathbf{z}}{dt} = \mathbf{L}_T(\mathbf{z}) + \mathbf{g}(\mathbf{z}) = \mathbf{L}_C(\mathbf{z}) + \mathbf{L}_D(\mathbf{z}) + \mathbf{g}(\mathbf{z}), \quad \mathbf{L}_T(\mathbf{z}) = \mathbf{L}_C(\mathbf{z}) + \mathbf{L}_D(\mathbf{z}) \quad (8)$$

where  $\mathbf{L}_C(\mathbf{z})$ ,  $\mathbf{L}_D(\mathbf{z})$  the spatial transport operators representing convection and diffusion, respectively, and  $\mathbf{L}_T(\mathbf{z})$  their sum. On condition that the timescales associated with the transport processes are slower than all fast chemical timescales ( $\tau_1, \dots, \tau_M$ ), according to the CSP theory, Eq. 8 can be written in a form equivalent to that in Eq. 7 as follows [75, 76]:

$$f^m \approx 0 \quad (m = 1, M) \quad \frac{d\mathbf{z}}{dt} \approx \sum_{n=M+1}^{N+1} \mathbf{a}_n f^n. \quad (9)$$

The only difference between Eq. 7 and Eq. 9 is that in the latter the amplitudes  $f^i$  take transport into account:

$$f^i = \mathbf{b}^i \cdot (\mathbf{L}_T(\mathbf{z}) + \mathbf{g}(\mathbf{z})). \quad (10)$$

By using the right ( $\boldsymbol{\alpha}_i$ ) and left ( $\boldsymbol{\beta}^i$ ) eigenvectors of the Jacobian  $\mathbf{J}$  of  $\mathbf{g}(\mathbf{z})$  as leading order approximations of  $\mathbf{a}_i$  and  $\mathbf{b}^i$ , respectively, Eq. 9 and 10 can be written in the form of Eqs. 11 and 12:

$$f^m \approx 0 \quad (m = 1, M) \quad \frac{d\mathbf{z}}{dt} \approx \sum_{n=M+1}^{N+1} \alpha_n f^n \quad (11)$$

$$f^i = \boldsymbol{\beta}^i \cdot (\mathbf{L}_T(\mathbf{z}) + \mathbf{g}(\mathbf{z})) = \sum_{j=1}^{N+1} \beta_j^i L_{T,j} + \sum_{k=1}^{2K} \boldsymbol{\beta}^i \cdot \hat{\mathbf{S}}_k R^k = \sum_{m=1}^{2K+N+1} \gamma_m^i. \quad (12)$$

The contribution of the  $k$ -th process (chemical or transport) to the amplitude of the  $n$ -th mode can be assessed by the amplitude participation index (API) tool ( $P_k^n$ ) [77–80]:

$$P_k^n = \frac{\gamma_k^n}{\sum_{j=1}^{2K+N+1} |\gamma_j^n|} \quad (13)$$

Obviously,  $\sum_{m=1}^{2K+N+1} |P_k^n| = 1$  for all  $n = 1, \dots, N+1$ . When  $P_k^n$  is positive, the  $k$ -th process tends to increase the amplitude of the  $n$ -th mode while the opposite applies when negative. By combining the API values of all chemical processes ( $k = 1, \dots, 2K$ ) for the  $n$ -th mode, the contribution of chemistry to the amplitude of the  $n$ -th mode can be assessed [54, 81]:

$$H_{Chem}^n = \sum_{k=1}^{2K} |P_k^n|. \quad (14)$$

In a similar manner, the total contributions of transport, diffusion and convection to the amplitude of the  $n$ -th mode can also be quantified, i.e.,  $H_{Tran}^n$ ,  $H_{Diff}^n$  and  $H_{Conv}^n$ . Therefore, by definition,  $H_{Tran}^n + H_{Chem}^n = 1$  and  $H_{Diff}^n + H_{Conv}^n + H_{Chem}^n = 1$ , for  $n=1, N+1$ .

75 In the current work it will be shown that the system's characteristic mode is the fast explosive one. Therefore, the discussion will focus on the explosive timescale  $\tau_{e,f}$ , the associated amplitude  $f^{e,f}$ , the largest API values  $P_k^{e,f}$  and the total contributions of the chemistry and diffusion to  $f^{e,f}$ , i.e.,  $H_{Chem}^{e,f}$  and  $H_{Diff}^{e,f}$ , respectively.

In addition, following the same practice as in [62, 63], the analysis will be performed from a Lagrangian perspective. Consequently, Eq. 8 will be considered in the form of Eq. 15:

$$\frac{D\mathbf{z}}{Dt} = \mathbf{L}_D(\mathbf{z}) + \mathbf{g}(\mathbf{z}) \quad (15)$$

80 where  $D(\cdot)/Dt$  is the total derivative operator. Hence, the right-hand-side of Eq. 15 considers the chemical source term  $\mathbf{g}(\mathbf{z})$  and the spatial operator of diffusion  $\mathbf{L}_D(\mathbf{z})$ .

For the heat release rate analysis, the spatially integrated total heat release rate  $Q$  will be calculated from Eq. 16:

$$Q = \int_x HRR(x) dx, \quad (16)$$

where HRR the local heat release rate value. In a similar manner, the total contribution  $c_i$  of the  $i$ -th reaction to the global heat release rate  $Q$  will be calculated from Eq. 17:

$$c_i = \frac{q_i}{Q}, \quad q_i = \int_x hrr_i(x) dx \quad (17)$$

where  $hrr_i$  the local heat release associated with the  $i$ -th reaction.

Finally, the effective Lewis number  $Le_{eff}$  will be calculated from the volume-based definition of Eq. 18 [82–84]:

$$Le_{eff} = x_{H_2} Le_{H_2} + x_{H_2O_2} Le_{H_2O_2} \quad (18)$$

where  $x_{H_2}$  and  $x_{H_2O_2}$  the upstream mole fractions of  $H_2$  and  $H_2O_2$ , respectively and  $Le_{H_2}$ ,  $Le_{H_2O_2}$  the Lewis number calculated on the basis of  $H_2$  and  $H_2O_2$ , respectively. It is noted that all results were found to be consistent with the diffusion-based definition of the effective Lewis number [83–85].

85 Since the current work follows up to the earlier study of Ref. [10], the chemical reaction mechanism of Aramco 3 [86] was employed in the current study, supplemented with the nitrogen mechanism of *Glarborg et al.* [87].

All simulations were performed using the Chemkin-Pro software [41] (freely propagating adiabatic pre-mixed laminar flame model), while the CSP analysis was performed using the CSPTk package [88] integrated  
 90 with the TChem package [89] for thermo-kinetic database management. In all simulated cases, the adaptive grid control based on solution curvature and gradient values were set to 0.1 or lower, the absolute and relative tolerances were set to  $10^{-9}$  and  $10^{-4}$ , respectively, and the domain’s size was 52 mm. In all cases, the domain’s size was sufficiently small to ensure that the mixture does not ignite. Additional tests were also performed to ensure that the obtained results do not depend on the size of the domain. In addition, unless  
 95 otherwise stated, mixture-averaged transport properties were used.

### 3. Results

#### 3.1. The effect of $H_2O_2$ addition on the flame structure and the laminar flame speed

The one-dimensional (1D) freely propagating premixed laminar flame simulations and the subsequent analysis were mainly performed at fuel lean ( $\phi = 0.5$ ), atmospheric conditions and  $T_u=300$  K, but the discussion with additional findings were extended to a higher temperature ( $T_u=600$  K) and pressure ( $p=30$  atm) which are more relevant to a compression ignition engine operation. For brevity, in the following, the case of  $p=1$  atm and  $T_u=300$  K, will be referred to as "*baseline*", the case of  $p=1$  atm and  $T_u=600$  K will be referred to as "*high T*" and the case of  $p=30$  atm and  $T_u=600$  K will be referred to as "*high p-T*".  $H_2O_2$  is added on the basis of the fuel mole fraction. Therefore, a 10% addition of  $H_2O_2$  implies that the  $H_2O_2$  mole fraction ( $X_{H_2O_2}$ ) comprises 10% of the total fuel ( $X_F = X_{H_2} + X_{H_2O_2}$ ) mole fraction, i.e.,  $X_{H_2O_2}/(X_{H_2} + X_{H_2O_2}) = 0.10$ . The addition of  $H_2O_2$  is performed in a way ensuring that the mixture’s upstream equivalence ratio, in accordance with the typical definition of  $\phi = (X_F/X_{air})/(X_F/X_{air})_{st}$ , is kept

fixed. However, this definition does not account for the fact that  $\text{H}_2\text{O}_2$  can act as oxidiser. For that purpose, the use of an effective equivalence ratio, as the one used in Ref. [90], may be more representative. Therefore, on the assumption that one mole of  $\text{H}_2\text{O}_2$  leads to the formation of 1 mol of  $\text{H}_2\text{O}$  and half mole of  $\text{O}_2$  the effective equivalence ratio is defined as:

$$\phi_{eff} = \frac{X_{\text{H}_2}/(0.5X_{\text{H}_2\text{O}_2} + X_{\text{O}_2})}{(X_{\text{H}_2}/X_{\text{O}_2})_{st}} \quad (19)$$

where the subscript *st* denotes stoichiometric conditions. In principle, the addition of  $\text{H}_2\text{O}_2$  will tend to shift the  $\phi_{eff}$  of the mixture towards stoichiometry while the opposite stands. However, as it will be shown next, this shifting is very small for the conditions under study.

Table 1 displays the reactions that are highlighted in the analysis next. The symbols “f” and “b” used next to the reaction numbers, stand for forward and backward, respectively. The reactions listed in Table 1 are those which are either identified by the API CSP tool to play a key role to the flame’s structure or to have large contribution to the heat release rate, in all the different cases that are analysed in the current section. These reactions will be discussed in detail next.

Table 1: The most significant reactions to the dynamics of the system in all examined cases. These reactions are either identified by the API CSP tool to play a key role to the flame’s structure or to have large contribution to the heat release rate, in all the different cases that are analysed and discussed in the current work.

2.	$\text{H}_2 + \text{O} \leftrightarrow \text{H} + \text{OH}$	11.	$\text{H}_2\text{O}_2 + \text{H} \leftrightarrow \text{H}_2 + \text{HO}_2$
3.	$\text{H}_2 + \text{OH} \leftrightarrow \text{H}_2\text{O} + \text{H}$	15.	$\text{HO}_2 + \text{H} \leftrightarrow 2\text{OH}$
5.	$\text{H} + \text{O}_2 \leftrightarrow \text{OH} + \text{O}$	16.	$\text{HO}_2 + \text{H} \leftrightarrow \text{H}_2 + \text{O}_2$
6.	$\text{H} + \text{OH} + \text{M} \leftrightarrow \text{H}_2\text{O} + \text{M}$	18.	$\text{HO}_2 + \text{OH} \leftrightarrow \text{H}_2\text{O} + \text{O}_2$
9.	$\text{H}_2\text{O}_2 (+\text{M}) \leftrightarrow 2\text{OH} (+\text{M})$	21.	$\text{H} + \text{O}_2 (+\text{M}) \leftrightarrow \text{HO}_2 (+\text{M})$
10.	$\text{H}_2\text{O}_2 + \text{H} \leftrightarrow \text{H}_2\text{O} + \text{OH}$		

One of the most important properties of laminar flames is the flame speed  $s_L$ . Figure 1a displays the laminar flame speed variation against the mixture’s equivalence ratio  $\phi$  at the *baseline* conditions for the case of no- and 10% addition of  $\text{H}_2\text{O}_2$ . It is shown that the addition of  $\text{H}_2\text{O}_2$  induces a significant increase to the laminar flame speed in the range of fuel-lean to fuel-rich mixtures. Although not explicitly shown, the flame speed increase at fuel lean conditions is larger than the respective increase at stoichiometric or fuel-rich conditions. For instance, at  $\phi = 0.5$ , 10% addition of  $\text{H}_2\text{O}_2$  induces 72% increase of the  $s_L$ , while the respective values at  $\phi = 1.0$  and 1.5 are 31% and 34%. Since the current work aims at fuel lean conditions, the discussion will continue on those without dismissing though the importance of the stoichiometric and fuel-rich conditions. The strong effect of  $\text{H}_2\text{O}_2$  addition on the laminar flame speed is also confirmed at the *high-T* and *high p-T* conditions, as it is displayed in Fig. 1b. In fact, the laminar flame speed increase is amplified significantly at the *high p-T* conditions, where 10%  $\text{H}_2\text{O}_2$  addition results in 140% increase of  $s_L$ . At all three sets of conditions the laminar flame speed change is roughly linear to the  $\text{H}_2\text{O}_2$  addition. Finally,

Fig. 1c demonstrates that at the fuel conditions of  $\phi = 0.5$ , the addition of  $\text{H}_2\text{O}_2$  leads to an increase of the effective equivalence ratio ( $\phi_{eff}$ ), which for the cases that will be investigated next (i.e., 5% and 10%  $\text{H}_2\text{O}_2$  addition), does not exceed the value of  $\sim 5\%$  compared to  $\phi$ .

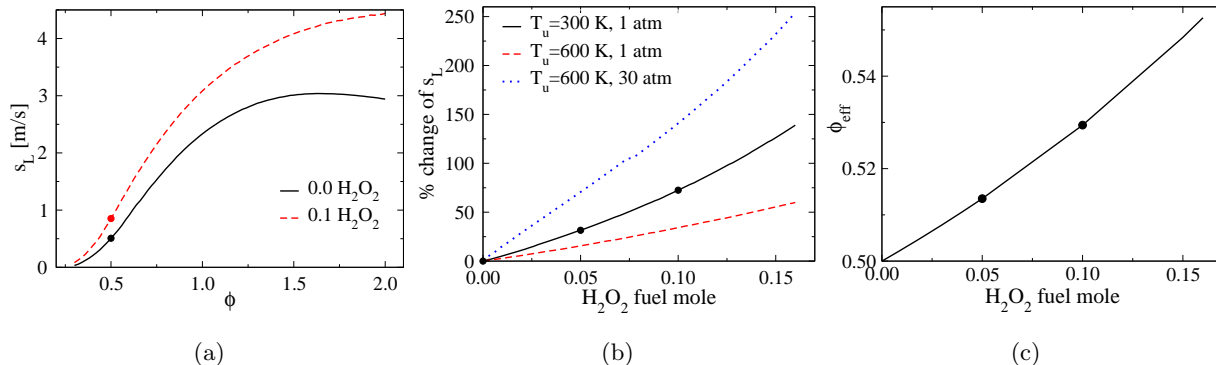


Figure 1: (a) Laminar flame speed calculations for a 1D freely propagating premixed hydrogen/air flame ( $T_u=300$  K,  $p=1$  atm) without any  $\text{H}_2\text{O}_2$  addition (black-solid line) and a 10%  $\text{H}_2\text{O}_2$  addition (red-dashed line) for a range of equivalence ratio ( $\phi$ ). (b) Percentage change of the laminar flame speed of a 1D freely propagating premixed hydrogen/air flame at  $\phi = 0.5$  due to the addition of  $\text{H}_2\text{O}_2$ , at three different conditions:  $T_u=300$  K,  $p=1$  atm (solid line),  $T_u=600$  K,  $p=1$  atm (dashed line),  $T_u=600$  K,  $p=30$  atm (dotted line). (c) The evolution of the effective equivalence ratio as a function of the addition of  $\text{H}_2\text{O}_2$ , for the laminar flames displayed in Fig. 1(b). For all figures: The filled symbols represent the cases analysed in detail next.

Before initiating the discussion on the effect of  $\text{H}_2\text{O}_2$  addition on the flame structure at the *baseline* conditions and discussing the respective changes in the CSP diagnostics, it is informative to briefly discuss the no- $\text{H}_2\text{O}_2$  case which will be used as a reference. It is noted that all results will be presented and discussed in the progress variable space, as represented by temperature, so that they can be readily compared with future turbulent combustion simulations. Starting with the species mass fraction profiles along with the heat release rate, both plotted in Fig. 2, it is shown that the flame zone can be roughly split into three regions: a low temperature zone where  $\text{HO}_2$  and  $\text{H}_2\text{O}_2$  reach maximum, followed by a mid-temperature and high heat release region that H and O rapidly increase, and completed by a high-temperature zone where OH reaches its maximum and maintains high values. These results are well documented in the literature (e.g., [91]). In addition, Fig. 2b also shows that the heat release rate reaches its maximum at  $\sim 1,050$  K and the largest contributors to its generation are: (i) the exothermic reactions 18 and 21 in the first low-temperature region, (ii) the exothermic reactions 21, 3, 15 and the endothermic reaction 5 in the mid-temperature region where the heat release exhibits its largest increase and (iii) the exothermic reactions 18 and 6 in the high-temperature region.

The  $N+1$  chemical timescales  $\tau_i$  (associated with the  $N+1$  CSP modes) that develop in the 0%  $\text{H}_2\text{O}_2$  case at the *baseline* conditions are displayed in Fig. 3. It is shown that all timescales are of dissipative nature except for two which are explosive: a fast  $\tau_{e,f}$  and a slow  $\tau_{e,s}$ . This indicates that  $N-1$  CSP modes are

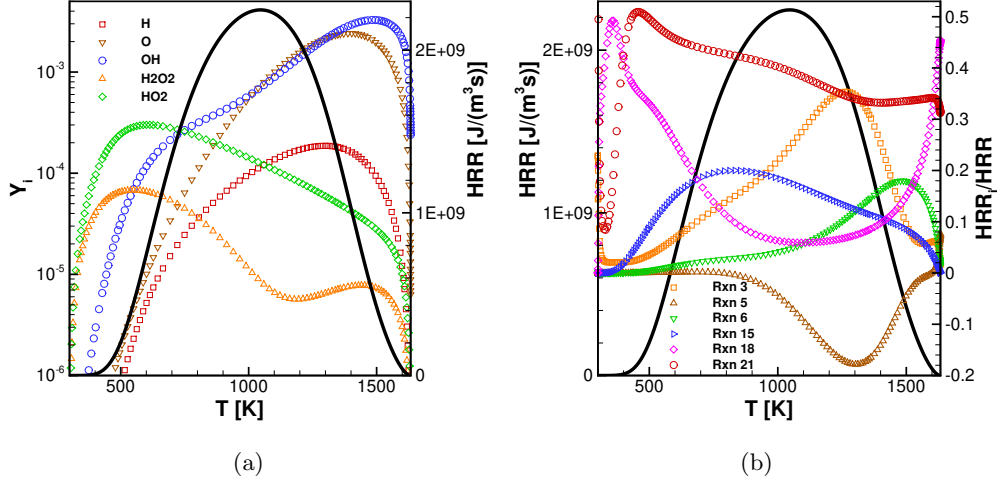


Figure 2: (a) Evolution of selected species mass fractions and the HRR (black-solid line) against temperature. (b) Evolution of the HRR (black-solid line) and the individual contributions of the reactions with largest effect on the HRR, against temperature. Both subfigures refer to the case of a freely propagating laminar premixed hydrogen/air flame ( $p=1$  atm,  $T_w=300$  K,  $\phi=0.5$ ).

dissipative while two modes are explosive. The fast explosive timescale  $\tau_{e,f}$  rapidly accelerates in the region of  $300 \text{ K} < T < 550 \text{ K}$ , from values in the order of  $10^3$  s to  $10^{-4}$  s. Therefore, it can be concluded that in this zone  
 150 the effect of  $\tau_{e,f}$  is small. At  $T \approx 550$  K,  $\tau_{e,f}$  starts exhibiting a moderate acceleration and a gap is established between  $\tau_{e,f}$  and the faster timescales indicating that a valid reduced model can be constructed. The fact that  $\tau_{e,f}$  is placed above the gap indicates that  $\tau_{e,f}$  is the faster of the slow timescales, hence one of the two conditions required to qualify for the system's characteristic one is met. The second condition, i.e., the dominance in the modes' amplitudes will be discussed next. At  $T \approx 700$  K a second explosive timescale  $\tau_{e,s}$   
 145 much slower than  $\tau_{e,f}$  emerges which gradually accelerates. At  $T \approx 1,090$  K  $\tau_{e,f}$  starts gradually decelerating, while  $\tau_{e,s}$  starts accelerating faster. At some point ( $T \approx 1,165$  K) the two explosive timescales meet and then disappear signifying the end of the *explosive stage* [44]. The disappearance of  $\tau_{e,f}$  and  $\tau_{e,s}$ , is due to the fact that the corresponding two positive eigenvalues, say  $\lambda_{e,f}$  and  $\lambda_{e,s}$ , meet, become a complex pair with positive real part and then evolve into a complex pair with a negative real part and finally to two negative real  
 150 eigenvalues [44]. The profile of  $\tau_{e,f}$  just described in the laminar flame configuration is qualitatively different from the respective in autoigniting systems where  $\tau_{e,f}$  exists from the very beginning of the process and most important, it typically exhibits a steep acceleration before it starts decelerating to meet  $\tau_{e,s}$  [45, 92].

As already explained, the system's characteristic mode must not only have an associated timescale among the fastest of the slow timescales but also the related amplitude must be dominant. Figure 3 indicated that  
 155 the fast explosive mode has an associated timescale  $\tau_{e,f}$  which is the fastest of the slow timescales. Table 2 lists the five largest CSP mode amplitudes at four representative spatial points which cover the whole breadth of the region where the fast explosive mode exists. It is noted that the mode number of the fast

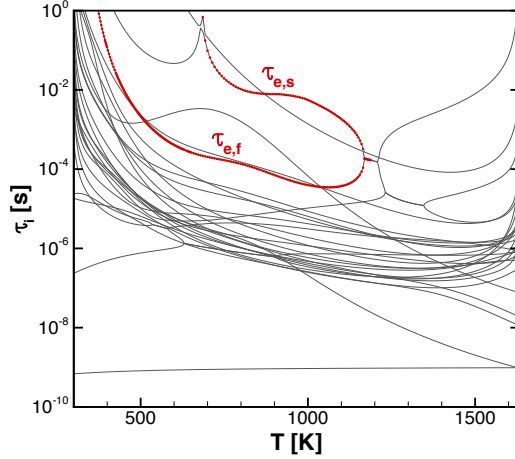


Figure 3: Evolution of the chemical time scales against temperature, in the case of a freely propagating laminar premixed hydrogen/air flame ( $p=1$  atm,  $T_u=300$  K,  $\phi=0.5$ ). Explosive/dissipative time scales are represented by red and black lines, respectively.

explosive mode changes across the flame because of the change in the ordering of the timescales as shown in Fig. 3, e.g., at the second point listed in Table 2 the fast explosive mode is the 25th mode while at the next point it has become the 23rd because two timescales became larger (slower) than that. In any case, the data listed in Table 2 are used to numerically demonstrate that the fast explosive mode's related amplitude  $h^{e,f}$  is by far the largest one in the area of interest, i.e., for  $T > 500$  K.

In summary, the developing timescales displayed in Fig. 3 and the largest CSP mode amplitudes provided in Table 2 demonstrate, respectively, that: (i)  $\tau_{e,f}$  is the fastest of the slow timescales and (ii)  $h^{e,f}$  is the largest of all amplitudes. Therefore, it can be concluded that the fast explosive mode is indeed the dominant one. For all the cases under study, the fast explosive mode was found to be the characteristic one in a manner similar to what was just discussed for the 0%-H<sub>2</sub>O<sub>2</sub> case at the *baseline* conditions.

Next, in Fig. 4 the  $H_{Chem}^{e,f}$  and  $H_{Diff}^{e,f}$  metrics, i.e., that is, the summative contributions of the chemistry and diffusion to the amplitude of the system's dominant mode, are compared against the  $\tau_{e,f}$  and HRR. It is reminded that by definition,  $H_{Chem}^{e,f} + H_{Diff}^{e,f} = 1$ . It is shown that  $H_{Chem}^{e,f} > H_{Diff}^{e,f}$  in the region of  $672K < T < 1,150K$  while  $H_{Chem}^{e,f} < H_{Diff}^{e,f}$  when  $300K < T < 672K$ . Therefore, from a system's dynamics perspective, the first region can be characterised as the *preheat zone* where diffusion prevails while the former as the *reaction zone* where the action of the chemical reactions becomes more important to the generation of  $f^{e,f}$ . In the following, any reference to these two zones will be performed on the basis of the aforementioned definitions. In addition, Fig. 4 further shows that in the *preheat zone*  $\tau_{e,f}$  exhibits a very steep acceleration indicating the the timeframe of action of the fast explosive mode becomes rapidly shorter, hence more active. In the *reaction zone*,  $\tau_{e,f}$  keeps accelerating but in more moderate fashion reaching values between  $3 \times 10^{-4}$ s to  $3 \times 10^{-5}$ s. A further comparison of the  $H_{Chem}^{e,f}$  with the HRR reveals that they are very well correlated with the only exception of the point in the progress variable space where they both reach their

Table 2: The largest amplitudes  $h^i$  of the CSP modes, at various spatial locations which cover the breadth of the region where the fast explosive mode exists (see  $\tau_{e,f}$  in Fig. 3), in a case of a freely propagating laminar premixed hydrogen/air flame;  $T_u=300\text{K}$ ,  $p=1$  atm,  $\phi=0.5$ . CSP modes in bold are the fastest explosive ones.

$\mathbf{x}$ [m]	0.00467	0.00478	0.00489	0.00503				
$\mathbf{T}$ [K]	320	393	637	1,053				
	i-th mode	$h^i$						
	<b>25:</b>	1.2E+05	<b>25:</b>	9.5E+05	<b>23:</b>	2.4E+06	<b>25:</b>	3.1E+06
	26:	4.5E+04	23:	4.1E+04	14:	5.0E+05	22:	1.0E+06
	22:	5.2E+03	26:	3.4E+04	26:	3.6E+05	27:	9.4E+05
	23:	1.7E+03	3:	3.5E+03	3:	2.8E+05	17:	9.5E+04
	28:	5.7E+02	2:	2.3E+03	10:	5.5E+04	13:	2.9E+04

180 maximum values:  $H_{Chem}^{e,f}$  reaches maximum at 927 K while the maximum of HRR is at 1,048 K. Yet, despite this small decorrelation, the region where the HRR reaches its highest value is characterised by high values of  $H_{Chem}^{e,f}$  as well. In terms of the individual processes that contribute to  $H_{Diff}^{e,f}$  and  $H_{Chem}^{e,f}$ , for the first, although it is not shown, the dominant contributor by more than 93% is the diffusion of heat while for the latter, the results are displayed in Fig. 4. Reactions 3f, 15f, 5f and 2f are the most important contributors favoring the increase of  $f^{e,f}$ , while the major opposition to its increase originates from 21f, 18f, 16f and 5b. These results are explained as follows. Reactions 2f, 5f, 15f are all chain branching reactions while 3f is a significant chain carrying step, hence all favor the radical pool generation. The importance of these reactions is well-documented in the literature [91]. On the other hand, reactions 21f and 5b compete reaction 5f, while reactions 16f and 18f are chain termination steps. As it will be shown next through the sensitivity analysis, 190 the reactions with large positive API values to  $f^{e,f}$  (e.g., 3f, 15f, 5f and 2f) tend to increase the laminar flame speed while the opposite applies for those with negative API values (e.g., 21f, 18f, 16f and 5b)

With the addition of  $\text{H}_2\text{O}_2$  at the *baseline* conditions, the fast explosive mode remains the dominant mode, its timescale being the fastest of the slow timescales and its amplitude being the largest. In fact, Fig. 5 shows that  $\tau_{e,f}$  becomes faster and  $f^{e,f}$  becomes larger, suggesting that the system's dominant mode becomes more active and its impact increases. It is noted though that the higher acceleration of  $\tau_{e,f}$  due to the addition of  $\text{H}_2\text{O}_2$  is mainly manifested at intermediate and high temperatures where it is expected that the chemistry will have more important role compared to diffusion. Notice also that  $\tau_{e,f}$  exists for higher progress variable values, thus extending the region in the progress variable space that affects the system's dynamics. The responses of  $\tau_{e,f}$  and  $f^{e,f}$  to the addition of  $\text{H}_2\text{O}_2$  at the *high T* and *high p-T* conditions are 195 very similar to those at the *baseline* conditions, therefore they are omitted.

Since  $f^{e,f}$  increases with the addition of  $\text{H}_2\text{O}_2$ , it is reasonable to investigate the processes that relate to this change. Firstly, Fig. 6 shows that the addition of  $\text{H}_2\text{O}_2$  increases the region in the progress variable space

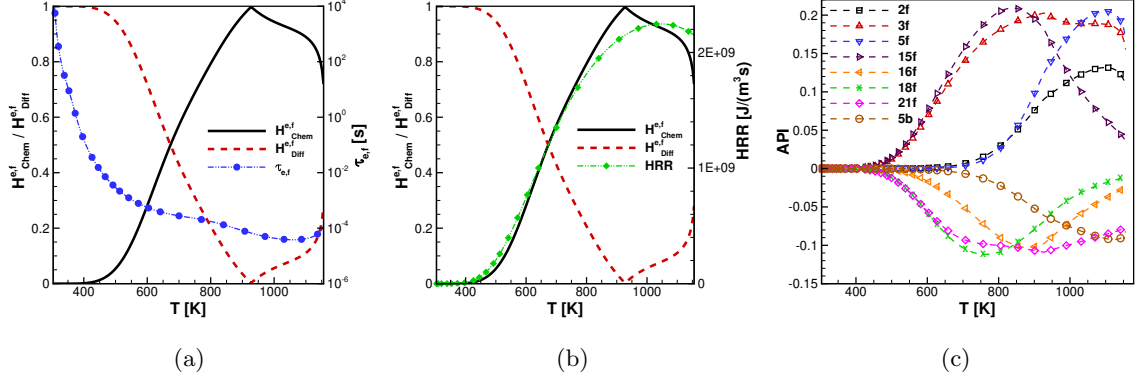


Figure 4: (a) Evolution of  $H_{Chem}^{e,f}$ ,  $H_{Diff}^{e,f}$  and  $\tau_{e,f}$  against temperature. (b) Evolution of  $H_{Chem}^{e,f}$ ,  $H_{Diff}^{e,f}$  and HRR against temperature. (c) Evolution of the reactions with the largest APIs related to the fast explosive mode against temperature. All subfigures refer to the case of a freely propagating laminar premixed hydrogen/air flame ( $p=1$  atm,  $T_u=300$  K,  $\phi=0.5$ ).

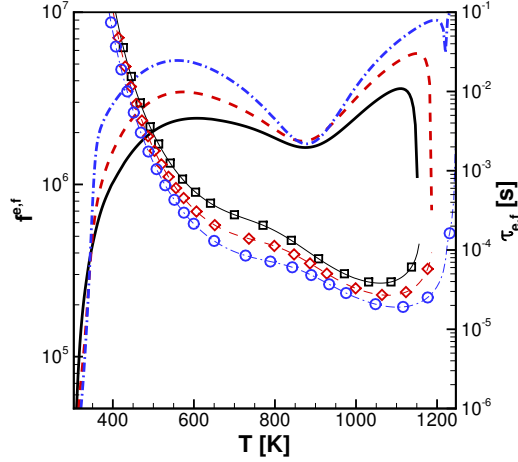


Figure 5: The evolution of the  $\tau_{e,f}$  and  $I^{e,f}$  against temperature, for the three cases of 0% (black-solid lines and square signs), 5% (red-dashed lines and diamond signs) and 10% (blue-dashed-dotted lines and circle signs)  $H_2O_2$  addition in the fuel (per vol). All cases refer to a freely propagating laminar premixed hydrogen/air flame ( $p=1$  atm,  $T_u=300$  K,  $\phi=0.5$ ).

where chemistry has a larger relative effect compared to diffusion, as this is manifested by the faster increase of  $H_{Chem}^{e,f}$  and the fact that  $\tau_{e,f}$  extends its presence in higher temperatures, as previously explained. It is reminded that  $H_{Chem}^{e,f} > H_{Diff}^{e,f}$  when  $H_{Chem}^{e,f} > 0.5$  (reaction zone) and  $H_{Chem}^{e,f} < H_{Diff}^{e,f}$  otherwise (preheat zone). Therefore, the reaction zone increases while the preheat zone decreases with the addition of  $H_2O_2$  in the progress variable space. This effect becomes more pronounced at the *high*  $p$ - $T$  conditions.

In order to appreciate in more detail the changes in the flame structure and identify the processes that are responsible for the reaction zone broadening, the API values of reactions with the largest contributions to  $I^{e,f}$  are next presented in Fig. 7 and 8 for the *baseline* and *high*  $p$ - $T$  conditions, respectively. Starting with the

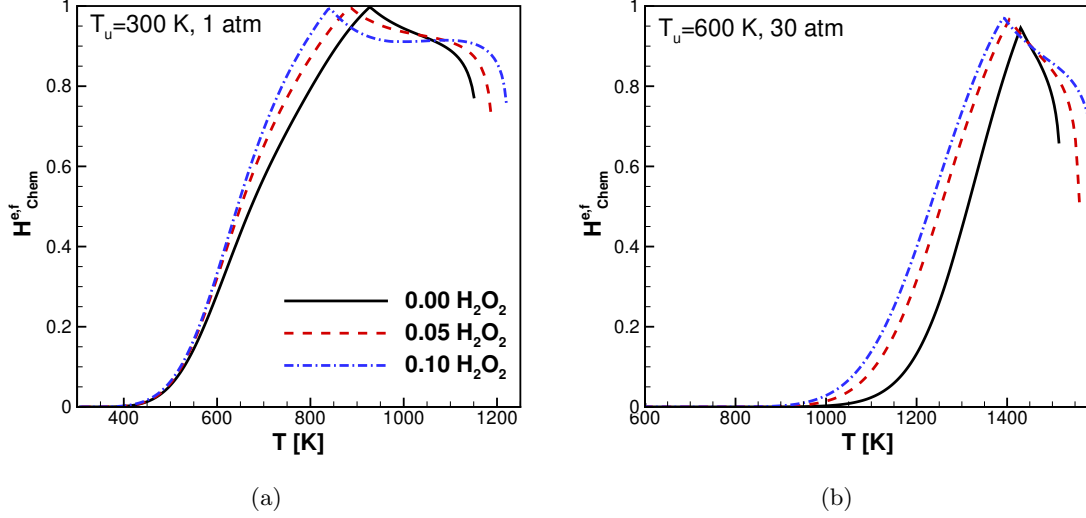


Figure 6: Evolution of  $H_{Chem}^{e,f}$  against temperature, for the three cases of 0% (black-solid line), 5% (red-dashed line) and 10% (blue-dashed-dotted line)  $H_2O_2$  addition in the fuel (per vol) at (a)  $p=1$  atm,  $T_u=300$  K and (b)  $p=30$  atm,  $T_u=600$  K. All cases refer to a freely propagating laminar premixed hydrogen/air flame ( $\phi=0.5$ ).

baseline conditions, Fig. 7 shows that the chemical process that is mostly affected by the addition of  $H_2O_2$  is reaction 10f, which from negligible API values in the 0% $H_2O_2$  case, it reaches a notable +7% in the 10% $H_2O_2$  case, favoring the increase of  $f^{e,f}$ . The notable rise in the relative importance of the H-abstraction reaction 10f is reasonable considering that it is a chain carrying reaction that includes  $H_2O_2$  as a reactant. However, the earlier increase of  $H_{Chem}^{e,f}$  and the subsequent broadening of the reaction zone after the addition of  $H_2O_2$  is also due to the earlier increase of reaction 3f which, favoring the increase of  $f^{e,f}$ , reaches higher API values. The earlier increase of reaction 3f is believed to be connected with the higher relative importance of reaction 10f, since reaction 3f depends on OH which is a product of reaction 10f. A non-negligible increase is also demonstrated in the API value of reaction 21f, which, unlike reactions 3f and 21f tends to decrease  $f^{e,f}$ . The increase of the relative importance of reaction 21f is associated with the enhanced effect of reaction 3f which produces H radicals essential for reaction 21f. The API values related to reactions 2f and 5f (both favoring the increase of  $f^{e,f}$ ) tend to start increasing for slightly higher temperatures and eventually their relative effect is increased after the addition of  $H_2O_2$ . The small suppression that reaction 5f experiences in the increase of its associated API value is due to the increased relative effect of the competing reaction 21f. The suppression of the relative effect of reaction 5f affects in turn the relative effect of reaction 2f. Finally, the API values related to reactions 15f, 16f and 18f (the first favoring and the latter two opposing the increase of  $f^{e,f}$ ) remain largely unaffected by the addition of  $H_2O_2$ . However, their role cannot be dismissed since they maintain their importance with notable relative contributions to  $f^{e,f}$ .

At the *high p-T* conditions, the changes in the flame structure in view of the largest contributors to  $f^{e,f}$  are more pronounced. Firstly, unlike the baseline conditions where the addition of  $H_2O_2$  was reflected

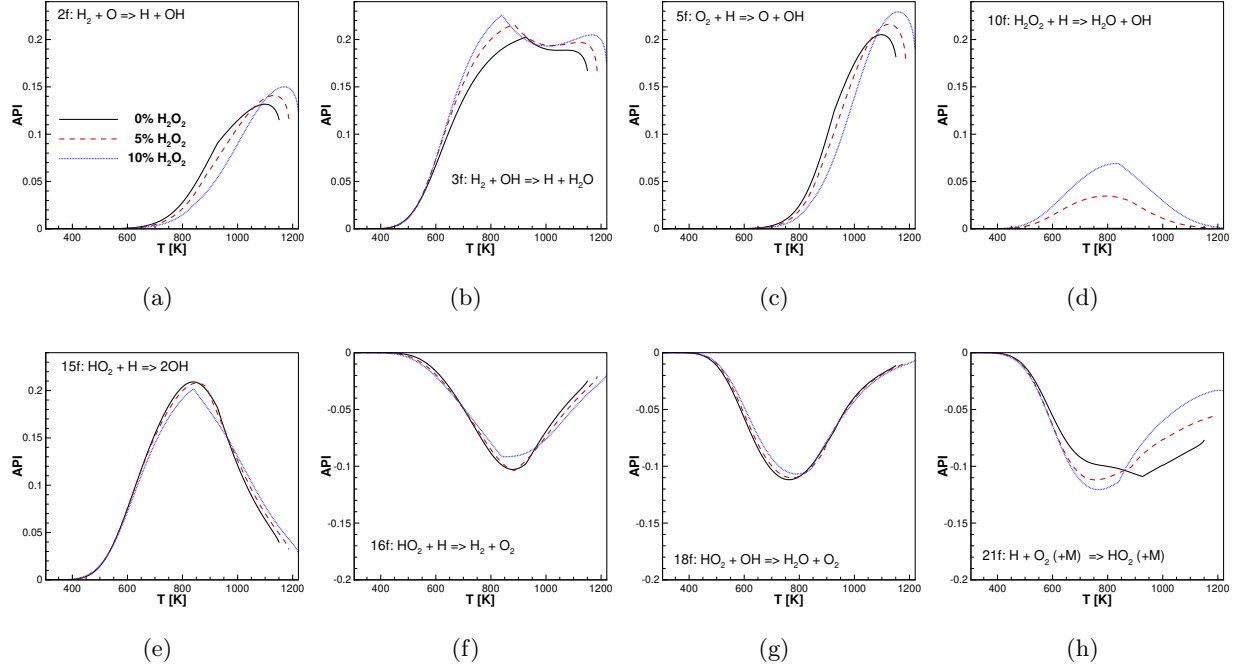


Figure 7: Evolution of the reactions with the largest APIs related to the fast explosive mode against temperature, for the three cases of 0% (black-solid lines), 5% (red-dashed lines) and 10% (blue-dotted lines)  $\text{H}_2\text{O}_2$  addition in the fuel (per vol). All cases refer to a freely propagating laminar premixed hydrogen/air flame ( $p=1$  atm,  $T_u=300$  K,  $\phi=0.5$ ).

to the importance of the  $\text{H}_2\text{O}_2$ -related reaction 10f, here, reaction 9f is favored instead (supporting the increase of  $f^{e,f}$ ) reaching higher maximum API value compared to the one attained by reaction 10f. The main reason probably that leads to the favor of reaction 9f instead of 10f at the *high*  $p$ - $T$  conditions relates to the associated higher activation energy  $E_a$ . Reaction 9f has an activation energy of  $E_a=4.8749\text{E}+04$  as opposed to  $E_a=3.97\text{E}+03$  for 10f. This suggests that reaction 10f is favored at lower temperatures, therefore explains why at the *baseline* conditions the relative importance of reaction 10f prevails over 9f. Another important point that needs to be addressed is that reaction 9f is a chain branching reaction, thus favoring a larger radical pool compared to the chain carrying 10f. The increase in the relative importance of reaction 9f triggers notable increase to the relative importance of reactions 3f and 15f, both favoring the increase of  $f^{e,f}$ . The increase of the relative effect of reactions 9f, 3f and 15f is the main reason for the pronounced reaction zone broadening previously reported in Fig. 6. Reactions 5f and 21f, which are competing processes (the first favoring and the latter opposing the increase of  $f^{e,f}$ ), both have API values which decrease in magnitude due to the addition of  $\text{H}_2\text{O}_2$ . The decreasing relative influence of these two reactions does not mean though that their absolute contributions decrease as well. In fact, although not shown, their absolute contributions to  $f^{e,f}$  increase but the contributions related to other reactions increase higher. Finally, the relative contribution of 18f in opposing the increase of  $f^{e,f}$  remains largely unaffected by the addition of  $\text{H}_2\text{O}_2$ .

In summary, at low temperature/pressure the addition of  $\text{H}_2\text{O}_2$  affects the flame structure by enhancing

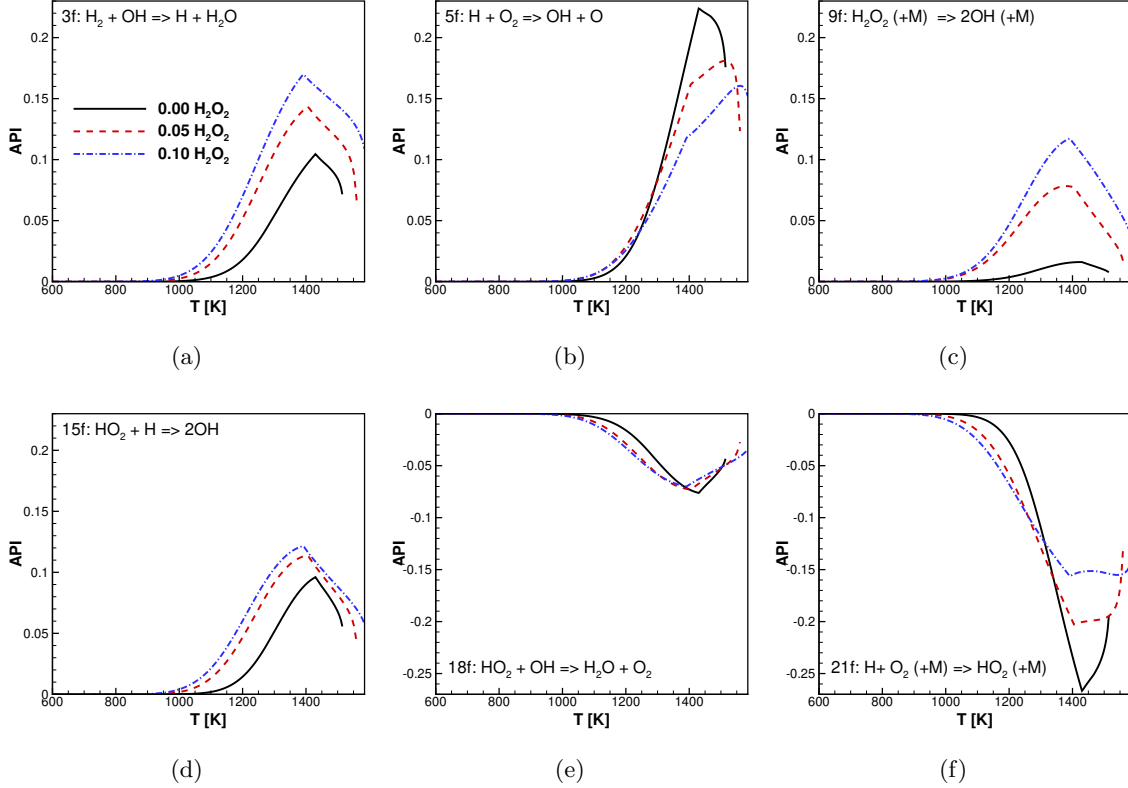


Figure 8: Evolution of the reactions with the largest APIs related to the fast explosive mode against temperature, for the three cases of 0% (black-solid lines), 5% (red-dashed lines) and 10% (blue-dotted lines)  $\text{H}_2\text{O}_2$  addition in the fuel (per vol). All cases refer to a freely propagating laminar premixed hydrogen/air flame ( $p=30$  atm,  $T_u=600$  K,  $\phi=0.5$ ).

the effect of the chain carrying reaction 10f which in turn enhances the influence of 3f. The pathway of  
 250 10f-3f is the main reason for the radical pool enhancement and the broadening of the reaction zone. The  
 enhancement of the relative contribution of 3f increases the effect of 21f, leading in turn to a small suppression  
 of the relative contribution of reaction 5f and subsequently that of reaction 2f. The relative contributions of  
 reactions 15f, 16f and 18f remain largely unaffected. At sufficiently high temperature/pressure the addition  
 of  $\text{H}_2\text{O}_2$  affects the flame structure primarily through reaction 9f. Compared to the chain carrying 10f the  
 255 chain branching 9f is more efficient in increasing the radical pool. The increased effect of reaction 9f causes  
 in turn a notable increase to the relative contributions of reactions 3f and 5f. The increased efficiency of the  
 chemical pathway of reactions 9f, 3f, 15f is the main reason for the broadening of the reaction as reflected  
 in the early increase of  $\text{H}_{Chem}^{e,f}$  due to the addition of  $\text{H}_2\text{O}_2$ . The relative contributions of the competing  
 reactions 5f and 21f decrease while that of reaction 18f remains largely unaffected.

260 Although chemistry plays an important role to the dynamics of the examined laminar flames, the role of  
 diffusion should not be dismissed. The fact that the laminar flames under study are lean hydrogen flames  
 enhances the significance of diffusion, due to the inherent non-equidiffusivity of such flames, reflected on the  
 Lewis number. The addition of  $\text{H}_2\text{O}_2$  in the hydrogen/air mixture necessitates the employment of an effective

Lewis number  $Le_{eff}$ , as the one described in Section 2. Figure 9 shows that the addition of  $H_2O_2$  leads to the increase of  $Le_{eff}$ , therefore favoring the thermodiffusive stability of the laminar flame. This finding is practically insensitive to the system’s initial conditions in terms of  $T_u$  and pressure. The decrease of the flame’s thermodiffusive instability after the addition of  $H_2O_2$  (as reflected to the increase of the effective Lewis number) is in agreement with the previously reported finding (Fig. 1c) that the  $H_2O_2$  addition leads to the increase of the effective equivalence ratio.

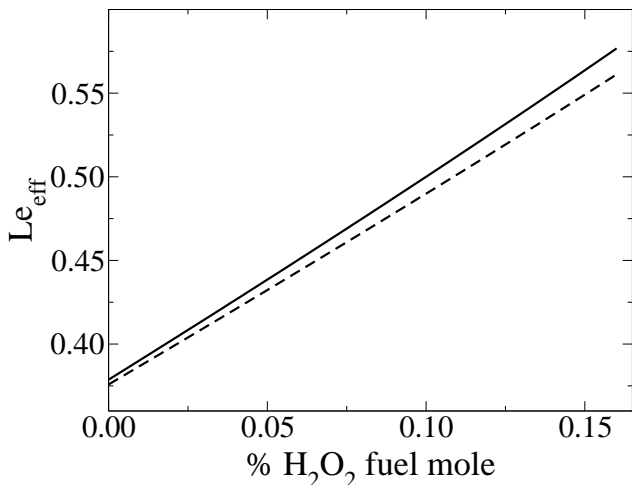


Figure 9: The mixture’s effective Lewis number as a function of the initial  $H_2O_2$  addition at  $T_u=300$  K (solid line) and 600 K (dashed line). All cases refer to a freely propagating laminar premixed hydrogen/air flame ( $p=1$  atm,  $\phi=0.5$ ).

To investigate further the non-unity Lewis number effect, additional cases at the *baseline* and *high p-T* conditions were simulated. The aim was to assess the dependence of the flame structure changes (due to the  $H_2O_2$  addition) on the flame’s non-equidiffusion characteristic. Figure 10 displays the evolution of  $H_{Chem}^{e,f}$  in the progress variable space for the 0% and 10%  $H_2O_2$  addition cases at the *baseline* and *high p-T* conditions. On top of these results has been overlaid the  $H_{Chem}^{e,f}$  evolution for the same conditions but with fixing Lewis number to 1. Firstly, it is shown that when  $Le=1$ , the addition of  $H_2O_2$  results again in a broadening of the reaction zone. However, in that case the reaction zone broadening becomes significantly decreased, becoming practically negligible both at the *baseline* and at *high p-T* conditions. These findings can be explained when the main mechanism that  $H_2O_2$  affects the flame structure is considered: the increase of the radical pool either through the pathways of 10f-3f (at the *baseline* conditions) or through 9f-3f-15f. The larger diffusivity of the reactants compared to the thermal diffusivity (i.e., in the non-unity Lewis number cases), becomes more effective in an enhanced radical pool, leading to the broadening of the reaction zone.

Following the same practice as in [59], a sensitivity analysis was performed in order to identify the reactions with the largest effect on the flame speed. The results were then compared against the set of reactions identified by the API tool on the basis of the system’s fast explosive mode. It is noted though

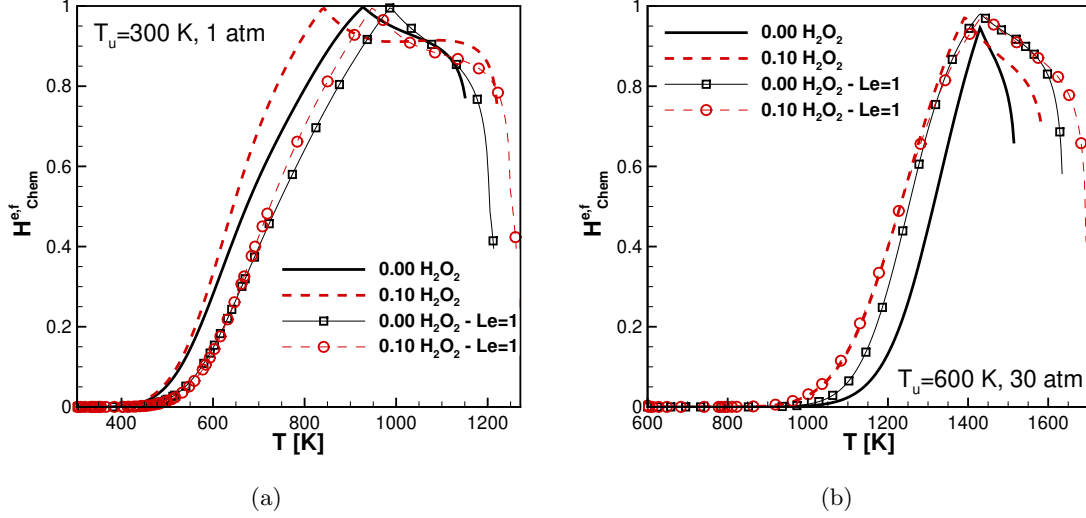


Figure 10: Evolution of  $H_{Chem}^{e,f}$  against temperature, for the cases of 0% (black-solid line) and 10% (red-dashed line)  $H_2O_2$  addition in the fuel (per vol) at (a)  $p=1$  atm,  $T_u=300$  K and (b)  $p=30$  atm,  $T_u=600$  K. All cases refer to a freely propagating laminar premixed hydrogen/air flame ( $\phi=0.5$ ).

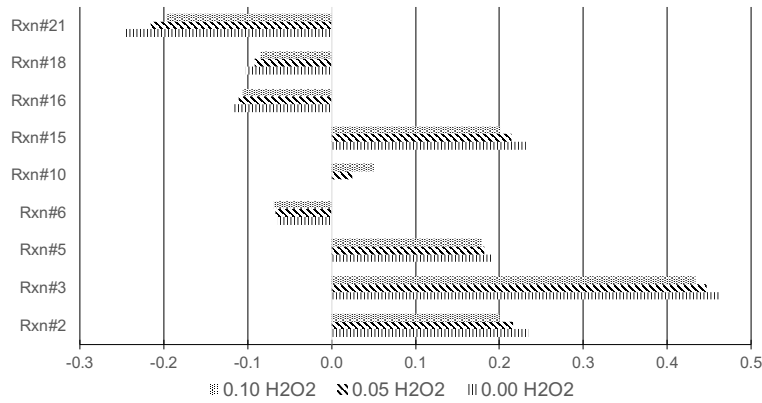
285 that the sensitivity indices have global character, i.e., characterise the whole flame, as opposed to the API values which are local and can vary significantly in a flame. As a result, the comparison between the two sets of reactions can only be qualitative. The results of the sensitivity analysis at the *baseline* and *high*  $p$ - $T$  conditions are displayed in Fig. 11 where the largest sensitivity coefficients are plotted for the 0%, 5% and 10% cases. It is shown that at the *baseline* conditions and 0% $H_2O_2$  case, the reaction with the largest effect on the flame speed is reaction 3 favoring its increase, followed by reactions 15, 2, 5 and 21, the first three favoring its increase while the latter tending to decrease the flame speed. Notable effect on the flame speed (but smaller in magnitude than the aforementioned ones) also have reactions 6, 16 and 18, all of them tending to decrease the flame speed. All these results are in agreement with previous sensitivity analyses at the same conditions [93]. When  $H_2O_2$  is added the same set of reactions remain the most important ones for the laminar flame speed in view of the sensitivity analysis indices with one exception: reaction 10 obtains considerable effect on the flame speed, favoring its increase. It is noted also that the  $H_2O_2$  addition leads to the decrease of the sensitivity indices of all reactions highlighted in the 0% $H_2O_2$  case, except for the index of reaction 6 which exhibits a small increase. A comparison of the set of the reactions identified as important by the API tool (Fig. 7) to those identified by the sensitivity analysis (Fig. 11a), reveals that: (i) all the reactions with large relative contributions to  $f^{e,f}$  have significant effect on the flame speed but the opposite applies for the vast majority and not all of the reactions, since reaction 6 has a non-negligible sensitivity index but its API value is small; (ii) the signs of the API values of the reactions identified as important contributors to the  $f^{e,f}$  are consistent with the signs of their respective sensitivity analysis indices, i.e., all reactions with large positive API values have notable positive sensitivity indices, therefore tend to increase the flame speed

290

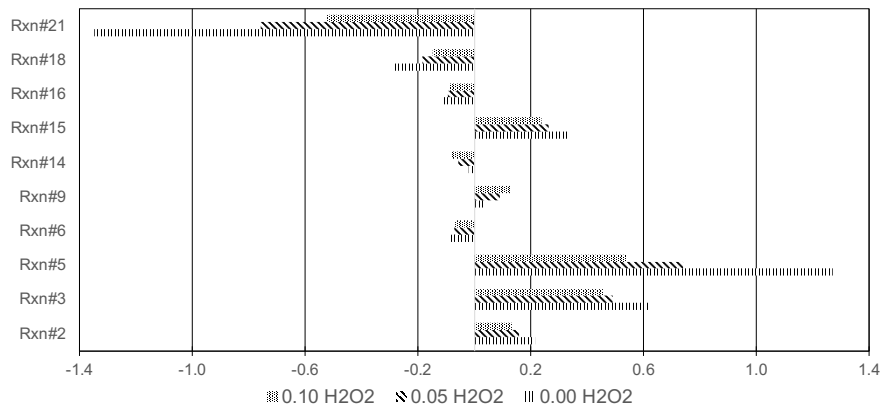
295

300

305 while the opposite holds for the reactions with the large negative API values. The aforementioned findings hold both at the *baseline* and *high p-T* conditions. In the latter, the reactions with the largest effect on the laminar flame speed are reactions 2, 3, 5 and 14 favoring its increase and reactions 6, 14, 16, 18 and 21 tending to decrease the magnitude of the flame speed. The aforementioned reactions are important both without any and with H<sub>2</sub>O<sub>2</sub> addition, with the only exception of reaction 9 which becomes important with  
 310 the addition of H<sub>2</sub>O<sub>2</sub>.



(a)



(b)

Figure 11: The reactions with the largest sensitivity coefficients against the flame speed for the three cases of 0%, 5% and 10% H<sub>2</sub>O<sub>2</sub> addition in the fuel, at (a) 1 atm, T<sub>u</sub>=300 K, (b) 1 atm, T<sub>u</sub>=600 K and (c) 30 atm, T<sub>u</sub>=600 K. All figures: all cases refer to a freely propagating laminar premixed hydrogen/air flame at  $\phi=0.5$ .

Additional insight on the changes induced by the addition of H<sub>2</sub>O<sub>2</sub> in the flame structure is also obtained by the investigation of the heat release metrics. In particular, the Q and c<sub>i</sub> metrics are used to provide a global insight since the first is the integrated (in the physical space) HRR while the latter reflects the relative contribution of each reaction to the aforementioned quantity of the integrated HRR. Figure 12 displays that  
 315 at the baseline conditions the addition of H<sub>2</sub>O<sub>2</sub> increases Q in a weakly non-linear manner. Indicatively, a

10% H<sub>2</sub>O<sub>2</sub> addition leads to ~100% increase of the integrated Q. The increase of Q is significant not only at the *baseline* but also at the *high T* and *high p-T* conditions. In fact, the increase of Q at the *high p-T* conditions is particularly amplified in agreement with what was previously reported for the increase of the laminar flame speed  $s_L$  (Fig. 1). A 10% of H<sub>2</sub>O<sub>2</sub> addition at the *high p-T* conditions yields a ~182% increase of the integrated heat release Q. The reaction with the largest contribution to Q that is mostly affected by the addition of H<sub>2</sub>O<sub>2</sub> at all three sets of conditions is reaction 21 with its relative effect being diminished. It is highlighted that the decreasing trend in the values of  $c_i$  for reaction 21 as a function of the addition of H<sub>2</sub>O<sub>2</sub> does not suggest that the heat release associated with reaction 21 decreases with the addition of H<sub>2</sub>O<sub>2</sub>. In fact, the  $q_i$  value of reaction 21 (i.e., the integrated heat release associated with reaction 21) increases with the addition of H<sub>2</sub>O<sub>2</sub>, but the increases of the  $q_i$  values associated with other reactions are stronger. In addition,  $c_{10}$  exhibits moderate increase of its relative contribution to Q at atmospheric conditions but its relative effect is mitigated at high pressure conditions. The relative effect of reaction 6 exhibits small increase at all three sets of conditions while the contributions of reactions 3, 15, 16 and 18 are largely unaffected by the addition of H<sub>2</sub>O<sub>2</sub>.

### 3.2. The effect of H<sub>2</sub>O<sub>2</sub> addition on NO<sub>x</sub> emissions

In the earlier work of Ref. [10], the effect of H<sub>2</sub>O<sub>2</sub> addition on the ignition delay time and NO<sub>x</sub> emissions of H<sub>2</sub>/air mixtures was investigated, in the context of an idealised homogeneous adiabatic batch reactor at compression ignition engine relevant conditions. Using CSP mathematical tools the chemical pathways that control the production of NO<sub>x</sub> were determined. One of the main findings to this regard was that H<sub>2</sub>O<sub>2</sub> addition results in a significant reduction in NO<sub>x</sub> emissions. This is opposite to the effect of H<sub>2</sub>O<sub>2</sub> addition on NO<sub>x</sub> emissions in the context of 1D freely propagating premixed laminar hydrogen/air flames, as displayed in Fig. 13, where it is shown that the H<sub>2</sub>O<sub>2</sub> addition results in substantial increase of NO in equilibrium, regardless the sets of conditions. Indicatively, a 10% addition of H<sub>2</sub>O<sub>2</sub> causes ~140% and ~400% increase of NO at the *baseline* and *high p-T* conditions, respectively. The main driver for the increase in the equilibrium mass fraction of NO is due to the temperature increase. This is a significant difference compared to the batch reactor simulations reported in Ref. [10] where it was found that the H<sub>2</sub>O<sub>2</sub> addition has negligible effect on the temperature. Here, it is shown that a 10% addition of H<sub>2</sub>O<sub>2</sub> at the *baseline* conditions leads to a ~10% increase in the equilibrium temperature, which is translated to ~156 K. At higher temperatures, the temperature increase due to the addition of H<sub>2</sub>O<sub>2</sub> is slightly mitigated but it reaches much higher values (for instance  $T_{eq}=2,000$  and 1,756 K at the *baseline* and *high p-T* conditions, respectively, for the 10% H<sub>2</sub>O<sub>2</sub> case), thus the effect of the temperature increase on the system (including NO<sub>x</sub>) becomes stronger. The reactions that have been found in the current work to be the most important contributors to the heat release increase, hence to the temperature increase, are summarised in Fig. 12. It is noted that similar increasing trends are observed for the mass fractions of the NO<sub>2</sub> and N<sub>2</sub>O pollutants. Finally, no qualitative changes were observed during the examination of the CSP diagnostics related to the key chemical pathways of the NO<sub>x</sub> pollutants, therefore, the reader is referred to [10] for a detailed description.

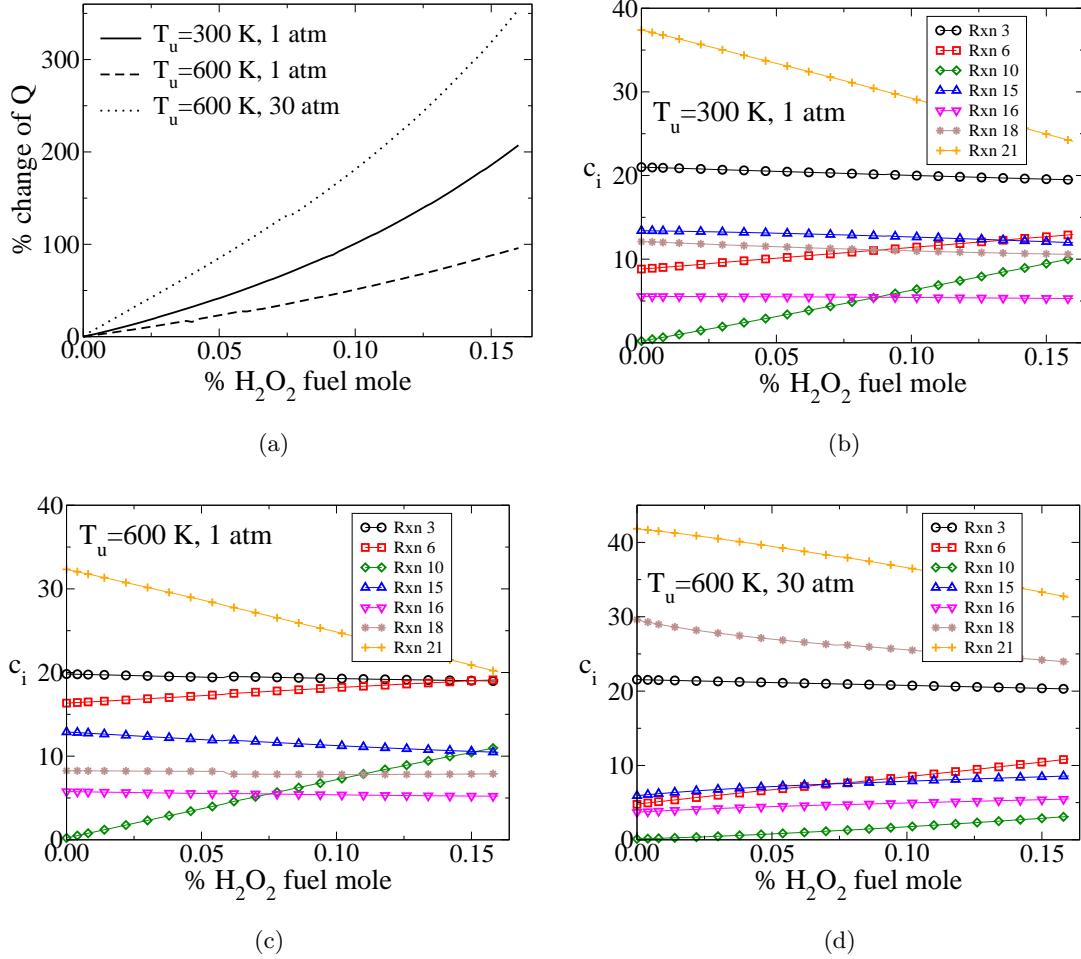


Figure 12: (a) The change in the integrated heat release  $Q$  as a function of the initial  $H_2O_2$  addition at three different sets of conditions:  $T_u=300$  K,  $p=1$  atm (solid line),  $T_u=600$  K,  $p=1$  atm (dashed line),  $T_u=600$  K,  $p=30$  atm (dotted line). The largest percentage contributors to the integrated heat release  $Q$  as a function of the initial  $H_2O_2$  addition at: (b) 1 atm,  $T_u=300$  K; (c) 1 atm,  $T_u=600$  K; (d) 30 atm,  $T_u=600$ . All figures: all cases refer to a freely propagating laminar premixed hydrogen/air flame at  $\phi=0.5$ .

#### 4. Conclusions

In the current work, the effect of hydrogen peroxide addition on the laminar flame speed, the flame structure and NOx emissions was investigated, in the context of a 1D freely propagating laminar premixed hydrogen/air flame at fuel lean conditions. The current work's key findings can be summarised as follows:

- hydrogen peroxide addition leads to a substantial increase of the laminar flame speed. Indicatively, a 10%  $H_2O_2$  (per fuel volume) addition results in 72% and 140% increase of the laminar flame speed at  $T_u=300$  K, 1 atm and  $T_u=600$  K, 30 atm, respectively.
- the reaction zone, as defined by the CSP diagnostics, is increased with the addition of  $H_2O_2$  due to

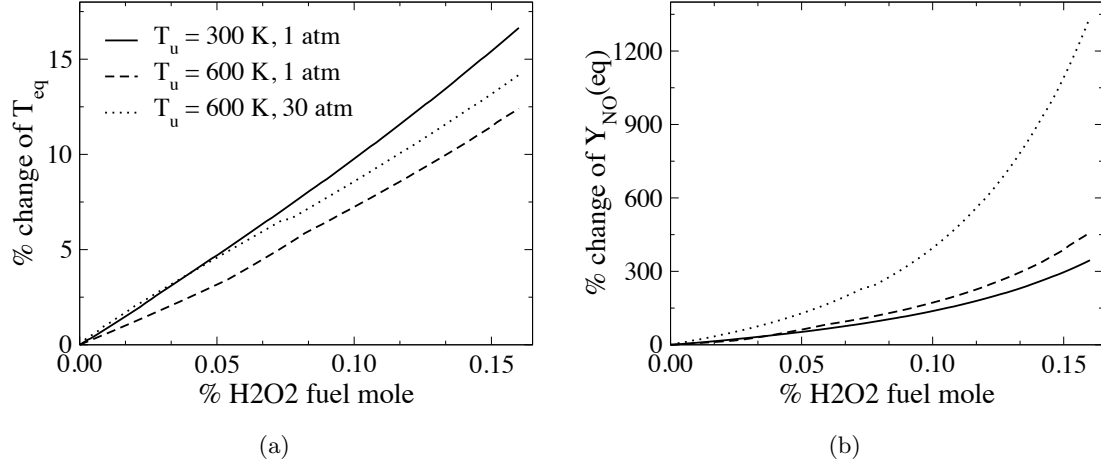


Figure 13: Percentage change of the equilibrium (a) temperature and (b) NO mass fraction, of a 1D freely propagating premixed hydrogen/air flame at  $\phi = 0.5$  due to the addition of  $H_2O_2$ , at three different conditions:  $T_u=300$  K,  $p=1$  atm (solid line),  $T_u=600$  K,  $p=1$  atm (dashed line),  $T_u=600$  K,  $p=30$  atm (dotted line).

360 the increased radical pool that is achieved.

- hydrogen peroxide addition alters the flame structure in a way that increases the importance of the chain carrying reaction (10f)  $H_2O_2 + H \rightarrow H_2O + OH$  or the chain branching reaction (9f)  $H_2O_2 (+M) \rightarrow 2OH (+M)$ , depending the conditions; the first is favored at low temperatures/pressures while the latter is favored at sufficiently high temperatures/pressures. The increased effect of reaction 10f enhances in turn the effect of reaction 3f ( $H_2 + OH \rightarrow H_2O + H$ ), while 9f increases the influence of reactions 3f and 15f ( $HO_2 + H \rightarrow 2OH$ ). The changes induced in these pathways are mainly responsible for the radical pool increase and the reaction zone broadening.

- hydrogen peroxide addition tends to make the laminar flame less thermodiffusively unstable as indicated by the increase of the effective Lewis number and the increase of the effective equivalence ratio.

- all the reactions identified as important by the CSP diagnostics have notable effect on the flame speed, as highlighted by the sensitivity analysis.

- hydrogen peroxide addition yields a large increase of the spatially integrated heat release. Indicatively, a 10% addition can lead to 100% and 182% increase at  $T_u=300$  K, 1 atm and  $T_u=600$  K, 30 atm, respectively.

- the reaction with the largest contribution to the integrated heat release that is mostly affected by the addition of  $H_2O_2$  is reaction 21 ( $H + O_2 (+M) \leftrightarrow HO_2 (+M)$ ), with its relative effect being diminished.

- hydrogen peroxide addition leads to a substantial increase of NO, opposite to what was reported in batch reactor simulations. Indicatively, a 10% addition of  $H_2O_2$  causes  $\sim 140\%$  and  $\sim 400\%$  increase of

NO at  $T_u=300$  K, 1 atm and  $T_u=600$  K, 30 atm, respectively. The increase of NO is associated with  
380 notable temperature increase.

Taking into account the results presented herein and in Ref. [10], the proposed technology of hydrogen/hydrogen peroxide blends in compression ignition engines seems to be a promising idea with good potential that deserves further exploration. However, further research is required that will showcase the potential of the proposed concept both through multidimensional simulations and experiments. The increased  
385 NOx emissions presented in the current work potentially pose an issue that needs to be addressed. To this regard, the dilution of the hydrogen/hydrogen peroxide mixture with steam might be an efficient approach. In fact, in the previous work of Ref. [10], steam dilution was reported to reduced NOx emissions by orders of magnitude. Besides, the use of steam for emissions' reduction purposes is a well documented and simple technique.

## 390 5. Acknowledgments

The current work has been supported by the Royal Society of Edinburgh (RSE) through the RSE/Scottish Government Sabbatical Research Grant scheme with grant no. 64676.

- [1] S. Verhelst, Recent progress in the use of hydrogen as a fuel for internal combustion engines, *Int. J. Hydrog. Energy* 39 (2) (2014) 1071–1085.
- 395 [2] S. Sharma, S. K. Ghoshal, Hydrogen the future transportation fuel: From production to applications, *Renew. Sust. Energ. Rev.* 43 (2015) 1151–1158.
- [3] M. Gurz, E. Baltacioglu, Y. Hames, K. Kaya, The meeting of hydrogen and automotive: a review, *Int. J. Hydrog. Energy* 42 (36) (2017) 23334–23346.
- [4] P. Moriarty, D. Honnery, Prospects for hydrogen as a transport fuel, *Int. J. Hydrog. Energy* 44 (31)  
400 (2019) 16029–16037.
- [5] A. L. Sánchez, F. A. Williams, Recent advances in understanding of flammability characteristics of hydrogen, *Prog. Energy Combust. Sci* 41 (2014) 1–55.
- [6] P. Dimitriou, T. Tsujimura, A review of hydrogen as a compression ignition engine fuel, *Int. J. Hydrog. Energy* 42 (38) (2017) 24470–24486.
- 405 [7] V. Chintala, K. Subramanian, A comprehensive review on utilization of hydrogen in a compression ignition engine under dual fuel mode, *Renew. Sust. Energ. Rev.* 70 (2017) 472–491.
- [8] A. A. Boretti, Novel heavy duty engine concept for operation dual fuel  $H_2-NH_3$ , *Int. J. Hydrog. Energy* 37 (9) (2012) 7869–7876.

- [9] N. Seignour, J. Masurier, B. Johansson, G. Dayma, P. Dagaut, F. Foucher, Ozone-assisted combustion  
410 of hydrogen: A comparison with isooctane, *Int. J. Hydrog. Energy* 44 (26) (2019) 13953–13963.
- [10] E.-A. Tingas, The chemical dynamics of hydrogen/hydrogen peroxide blends diluted with steam at  
compression ignition relevant conditions, *Fuel* 296 (2021) 120594.
- [11] W. Hertzelle, M. Waite, Design of a small H<sub>2</sub>O<sub>2</sub>/HTPB hybrid sounding rocket motor, in: 34th  
Aerospace Sciences Meeting and Exhibit, 1996, p. 8.
- 415 [12] T. Jacks, M. Beisler, Expanding hydrogen peroxide propulsion test capability at NASA’s Stennis Space  
Center E-Complex, in: 39th AIAA/ASME/SAE/ASEE Joint Propulsion Conference and Exhibit, 2003,  
p. 5041.
- [13] R. Amri, T. Rezoug, Numerical study of liquid propellants combustion for space applications, *Acta  
Astronaut.* 69 (7-8) (2011) 485–498.
- 420 [14] G. Glivin, V. Sreeja, Development of hydrogen peroxide based propellant systems for increasing energy  
efficiency, in: 2019 International Conference on Recent Advances in Energy-efficient Computing and  
Communication (ICRAECC), IEEE, 2019, pp. 1–4.
- [15] M. H. Morsy, Ignition control of methane fueled homogeneous charge compression ignition engines using  
additives, *Fuel* 86 (4) (2007) 533–540.
- 425 [16] M. H. Morsy, Modeling study on the production of hydrogen/syngas via partial oxidation using a  
homogeneous charge compression ignition engine fueled with natural gas, *Int. J. Hydrog. Energy* 39 (2)  
(2014) 1096–1104.
- [17] C. Born, N. Peters, Reduction of soot emission at a di diesel engine by additional injection of hydrogen  
peroxide during combustion, in: SAE Tech. Pap., SAE International, 1998. doi:10.4271/982676.
- 430 [18] B. Fanz, P. Roth, Injection of a H<sub>2</sub>O<sub>2</sub>/water solution into the combustion chamber of a direct injection  
diesel engine and its effect on soot removal, *Proc. Combust. Inst.* 28 (1) (2000) 1219–1225.
- [19] K. A. Subramanian, A. Ramesh, Use of hydrogen peroxide to improve the performance and reduce  
emissions of a ci engine fuelled with water diesel emulsions, in: SAE Tech. Pap., SAE International,  
2008.
- 435 [20] M. Ashok, C. Saravanan, Role of hydrogen peroxide in a selected emulsified fuel ratio and comparing it  
to diesel fuel, *Energ. Fuels* 22 (3) (2008) 2099–2103.
- [21] A. Demirci, H. Koten, M. Gumus, The effects of small amount of hydrogen addition on performance  
and emissions of a direct injection compression ignition engine, *Therm. Sci.* 22 (3) (2018) 1395–1404.

- 440 [22] J.-K. Yeom, S.-H. Jung, J.-H. Yoon, An experimental study on the application of oxygenated fuel to diesel engines, *Fuel* 248 (2019) 262–277.
- [23] B. M. Krishna, Experimental investigation on CI engine with hydrogen peroxide as an alternate, *Global Journal of Research In Engineering*.
- [24] A. T. Khalil, D. M. Manias, E.-A. Tingas, D. C. Kyritsis, D. A. Goussis, Algorithmic analysis of chemical dynamics of the autoignition of  $\text{NH}_3\text{-H}_2\text{O}_2/\text{air}$  mixtures, *Energies* 12 (23) (2019) 4422.
- 445 [25] S. H. Lam, D. A. Goussis, Understanding complex chemical kinetics with Computational Singular Perturbation, *Proc. Combust. Inst.* 22 (1989) 931–941.
- [26] S. H. Lam, D. A. Goussis, Conventional asymptotics and Computational Singular Perturbation for simplified kinetics modelling, in: M. O. Smooke (Ed.), *Reduced kinetic mechanisms and asymptotic approximations for methane-air flames*, no. 384 in Springer Lecture Notes, Springer-Verlag, Berlin, 450 1991, pp. 227–242.
- [27] S. H. Lam, D. A. Goussis, CSP method for simplifying kinetics, *Int. J. Chem. Kinet.* 26 (4) (1994) 461–486.
- [28] D. J. Diamantis, D. C. Kyritsis, D. A. Goussis, The reactions favoring or opposing the development of explosive modes: auto-ignition of a homogeneous methane/air mixture, *Proc. Combust. Inst.* 35 (2015) 455 267–274.
- [29] M. Valorani, D. A. Goussis, Explicit time-scale splitting algorithm for stiff problems: auto-ignition of gaseous mixtures behind a steady shock, *J. Comput. Phys.* 169 (1) (2001) 44–79.
- [30] D. A. Goussis, G. Skevis, Nitrogen chemistry controlling steps in methane-air premixed flames, in: K. J. Bathe (Ed.), *Comp. Fluid Solid Mech.*, Elsevier, Amsterdam, 2005, pp. 650–653.
- 460 [31] A. Massias, D. Diamantis, E. Mastorakos, D. Goussis, An algorithm for the construction of global reduced mechanisms with CSP data, *Combust. Flame* 117 (4) (1999) 685–708.
- [32] J. C. Lee, H. N. Najm, S. Lefantzi, J. Ray, M. Frenklach, M. Valorani, D. A. Goussis, On chain branching and its role in homogeneous ignition and premixed flame propagation, in: K. J. Bathe (Ed.), *Computational Fluid and Solid Mechanics*, Elsevier, Amsterdam, 2005, pp. 717–720.
- 465 [33] H. N. Najm, M. Valorani, D. A. Goussis, J. Prager, Analysis of methane-air edge flame structure, *Combust. Theor. Model.* 14 (2) (2010) 257–294.
- [34] M. Valorani, H. N. Najm, D. A. Goussis, CSP analysis of a transient flame-vortex interaction: Time scales and manifolds, *Combust. Flame* 134 (1-2) (2003) 35–53.

- [35] P. Pal, M. Valorani, P. G. Arias, H. G. Im, M. S. Wooldridge, P. P. Ciottoli, R. M. Galassi, Computational characterization of ignition regimes in a syngas/air mixture with temperature fluctuations, Proc. Combust. Inst. 36 (3) (2017) 3705–3716.
- [36] S. Gupta, H. G. Im, M. Valorani, Classification of ignition regimes in HCCI combustion using computational singular perturbation, Proc. Combust. Inst. 33 (2) (2011) 2991–2999.
- [37] S. Gupta, H. G. Im, M. Valorani, Analysis of n-heptane auto-ignition characteristics using computational singular perturbation, Proc. Combust. Inst. 34 (1) (2013) 1125–1133.
- [38] M. Valorani, F. Creta, P. Ciottoli, R. M. Galassi, D. Goussis, H. Najm, S. Paolucci, H. G. Im, E.-A. Tingas, D. Manias, et al., Computational singular perturbation method and tangential stretching rate analysis of large scale simulations of reactive flows: Feature tracking, time scale characterization, and cause/effect identification. part 1, basic concepts, in: Data analysis for direct numerical simulations of turbulent combustion, Springer International Publishing, 2020, pp. 43–64.
- [39] M. Valorani, F. Creta, P. Ciottoli, R. M. Galassi, D. Goussis, H. Najm, S. Paolucci, H. G. Im, E.-A. Tingas, D. Manias, et al., Computational singular perturbation method and tangential stretching rate analysis of large scale simulations of reactive flows: Feature tracking, time scale characterization, and cause/effect identification. part 2, analyses of ignition systems, laminar and turbulent flames, in: Data analysis for direct numerical simulations of turbulent combustion, Springer International Publishing, 2020, pp. 65–88.
- [40] R. J. Kee, J. F. Grcar, M. D. Smooke, J. A. Miller, E. Meeks, Premix: a fortran program for modeling steady laminar one-dimensional premixed flames, Sandia National Laboratories Report (SAND85-8249).
- [41] A. CHEMKIN-PRO, 18.0, ANSYS Reaction Design: San Diego.
- [42] T. Poinso, D. Veynante, Theoretical and numerical combustion, RT Edwards, Inc., 2005.
- [43] D. A. Goussis, Quasi steady state and partial equilibrium approximations: their relation and their validity, Combust. Theor. Model. 16 (5) (2012) 869–926.
- [44] D. J. Diamantis, E. Mastorakos, D. A. Goussis, H<sub>2</sub>/air autoignition: The nature and interaction of the developing explosive modes, Combust. Theor. Model. 19 (2015) 382–433.
- [45] E. A. Tingas, D. M. Manias, S. M. Sarathy, D. A. Goussis, CH<sub>4</sub>/air homogeneous autoignition: A comparison of two chemical kinetics mechanisms, Fuel 223 (2018) 74–85.
- [46] D. M. Manias, E. A. Tingas, C. E. Frouzakis, K. Boulouchos, D. A. Goussis, The mechanism by which CH<sub>2</sub>O and H<sub>2</sub>O<sub>2</sub> additives affect the autoignition of CH<sub>4</sub>/air mixtures, Combust. Flame 164 (2016) 111–125.

- 500 [47] E. A. Tingas, D. C. Kyritsis, D. A. Goussis, Autoignition dynamics of DME/air and EtOH/air homogeneous mixtures, *Combust. Flame* 162 (9) (2015) 3263–3276.
- [48] J. Lee, H. Najm, S. Lefantzi, J. Ray, M. Frenklach, M. Valorani, D. Goussis, A CSP and tabulation-based adaptive chemistry model, *Combust. Theor. Model.* 11 (1) (2007) 73–102.
- [49] E.-A. Tingas, D. J. Diamantis, D. A. Goussis, Issues arising in the construction of qssa mechanisms: the case of reduced n-heptane/air models for premixed flames, *Combust. Theor. Model.* 22 (6) (2018) 1049–1083.
- 505 [50] D. A. Goussis, H. G. Im, H. N. Najm, S. Paolucci, M. Valorani, The origin of CEMA and its relation to CSP, *Combust. Flame* 227 (2021) 396–401.
- [51] N. Sharmin, E.-A. Tingas, Dynamics analysis of a jet-fuel surrogate and development of a skeletal mechanism for computational fluid dynamic applications, *J. Energy Eng.* 146 (6) (2020) 04020064.
- 510 [52] K. K. Yalamanchi, E.-A. Tingas, H. G. Im, S. M. Sarathy, Screening gas-phase chemical kinetic models: Collision limit compliance and ultrafast timescales, *Int. J. Chem. Kinet.* 52 (9) (2020) 599–610. doi: 10.1002/kin.21373.
- [53] Y. Li, A. Alfazazi, B. Mohan, E. A. Tingas, J. Badra, H. G. Im, S. M. Sarathy, Development of a reduced four-component (toluene/n-heptane/iso-octane/ethanol) gasoline surrogate model, *Fuel* 247 (2019) 164–178.
- 515 [54] W. Song, E.-A. Tingas, H. G. Im, A computational analysis of methanol autoignition enhancement by dimethyl ether addition in a counterflow mixing layer, *Combust. Flame* 195 (2018) 84–98.
- [55] E. Singh, E.-A. Tingas, D. Goussis, H. G. Im, S. M. Sarathy, Chemical ignition characteristics of ethanol blending with primary reference fuels, *Energ. Fuel.* 33 (10) (2019) 10185–10196.
- 520 [56] S. M. Sarathy, E.-A. Tingas, E. F. Nasir, A. Detogni, Z. Wang, A. Farooq, H. Im, Three-stage heat release in n-heptane auto-ignition, *Proc. Combust. Inst.* 37 (1) (2019) 485–492.
- [57] M. Jaasim, E.-A. Tingas, F. E. H. Pérez, H. G. Im, Computational singular perturbation analysis of super-knock in SI engines, *Fuel* 225 (2018) 184–191.
- 525 [58] H. N. Najm, M. Valorani, D. A. Goussis, J. Prager, Analysis of methane–air edge flame structure, *Combust. Theor. Model.* 14 (2) (2010) 257–294.
- [59] J. Prager, H. N. Najm, M. Valorani, D. Goussis, Structure of n-heptane/air triple flames in partially-premixed mixing layers, *Combust. Flame* 158 (11) (2011) 2128–2144.
- [60] D. Manias, A.-E. Tingas, F. E. Hernandez Perez, H. G. Im, R. M. Galassi, P. P. Ciottoli, M. Valorani, Analysis of hydrogen/air turbulent premixed flames at different Karlovitz numbers using computational singular perturbation, in: *AIAA Aerospace Sciences Meeting*, 2018, p. 0364.
- 530

- [61] D. M. Manias, A.-E. Tingas, H. G. Im, Y. Minamoto, Dynamics analysis of a turbulent methane flame in mild combustion conditions, in: AIAA Scitech Forum, 2019, p. 1731.
- [62] D. M. Manias, E.-A. Tingas, F. E. H. Pérez, R. M. Galassi, P. P. Ciottoli, M. Valorani, H. G. Im, 535 Investigation of the turbulent flame structure and topology at different Karlovitz numbers using the tangential stretching rate index, *Combust. Flame* 200 (2019) 155–167.
- [63] D. M. Manias, E.-A. Tingas, Y. Minamoto, H. G. Im, Topological and chemical characteristics of turbulent flames at mild conditions, *Combust. Flame* 208 (2019) 86–98.
- [64] F. E. Hernandez Perez, H. G. Im, A. E. Tingas, Computational investigation of rod-stabilized laminar 540 premixed hydrogen–methane–air flames, in: AIAA Scitech Forum, 2020, p. 1659.
- [65] D. G. Patsatzis, D. A. Goussis, A new Michaelis-Menten equation valid everywhere multi-scale dynamics prevails, *Math. Biosci.* 315 (2019) 108220.
- [66] D. G. Patsatzis, D. T. Maris, D. A. Goussis, Asymptotic analysis of a target-mediated drug disposition model: algorithmic and traditional approaches, *Bull. Math. Biol.* 78 (6) (2016) 1121–1161.
- [67] M. Valorani, P. P. Ciottoli, R. M. Galassi, S. Paolucci, T. Grenga, E. Martelli, Enhancements of the 545 G-scheme framework, *Flow Turbul. Combust.* 101 (4) (2018) 1023–1033.
- [68] A. S. AlRamadan, R. M. Galassi, P. P. Ciottoli, M. Valorani, S. M. Sarathy, Multi-stage heat release in lean combustion: Insights from coupled tangential stretching rate (TSR) and computational singular perturbation (CSP) analysis, *Combust. Flame* 219 (2020) 242–257.
- [69] P. P. Ciottoli, R. M. Galassi, L. Angelilli, A. Cuoci, H. G. Im, M. Valorani, Analysis of wall–flame 550 interaction in laminar non-premixed combustion, *Combust. Sci. Techn.* (2019) 1–14.
- [70] Z. Li, R. M. Galassi, P. P. Ciottoli, A. Parente, M. Valorani, Characterization of jet-in-hot-coflow flames using tangential stretching rate, *Combust. Flame* 208 (2019) 281–298.
- [71] E.-A. Tingas, Z. Wang, S. M. Sarathy, H. G. Im, D. A. Goussis, Chemical kinetic insights into the 555 ignition dynamics of n-hexane, *Combust. Flame* 188 (2018) 28–40.
- [72] E. A. Tingas, H. G. Im, D. C. Kyritsis, D. A. Goussis, The use of CO<sub>2</sub> as an additive for ignition delay and pollutant control in CH<sub>4</sub>/air autoignition, *Fuel* 211 (2018) 898–905.
- [73] E.-A. Tingas, D. C. Kyritsis, D. A. Goussis, Comparative investigation of homogeneous autoignition of DME/air and EtOH/air mixtures at low initial temperatures, *Combust. Theor. Model.* 21 (1) (2017) 560 93–119.
- [74] E. A. Tingas, D. C. Kyritsis, D. A. Goussis, Ignition delay control of DME/air and EtOH/air homogeneous autoignition with the use of various additives, *Fuel* 169 (2016) 15–24.

- [75] M. Hadjinicolaou, D. A. Goussis, Asymptotic solution of stiff PDEs with the CSP method: the reaction diffusion equation, *SIAM J. Sci. Comput.* 20 (1998) 781–810.
- 565 [76] D. A. Goussis, M. Valorani, F. Creta, H. N. Najm, Reactive and reactive-diffusive time scales in stiff reaction-diffusion systems, *Prog. Comput. Fluid Dy.* 5 (6) (2005) 316–326.
- [77] D. Goussis, S. Lam, A study of homogeneous methanol oxidation kinetics using CSP, in: *Proc. Combust. Inst.*, Vol. 24, Elsevier, 1992, pp. 113–120.
- [78] E. A. Tingas, D. C. Kyritsis, D. A. Goussis, Algorithmic determination of the mechanism through  
570 which H<sub>2</sub>O-dilution affects autoignition dynamics and NO formation in CH<sub>4</sub>/air mixtures, *Fuel* 183 (2016) 90–98.
- [79] D. G. Patsatzis, E.-A. Tingas, D. A. Goussis, S. M. Sarathy, Computational singular perturbation analysis of brain lactate metabolism, *PloS one* 14 (12) (2019) e0226094.
- [80] A. T. Khalil, D. M. Manias, D. C. Kyritsis, D. A. Goussis, NO formation and autoignition dynamics  
575 during combustion of H<sub>2</sub>O-diluted NH<sub>3</sub>/H<sub>2</sub>O<sub>2</sub> mixtures with air, *Energies* 14 (1) (2021) 84.
- [81] D. Goussis, G. Skevis, E. Mastorakos, On transport-chemistry interactions in laminar premixed methane-air flames, in: *Proc. Int. Conf. Comput. Methods Sci. Engineer.*, ICCMSE'04, Vol. 1, Brill Academic Publishers, 2004, pp. 190–193.
- [82] S. Muppala, M. Nakahara, N. Aluri, H. Kido, J. Wen, M. Papalexandris, Experimental and analytical  
580 investigation of the turbulent burning velocity of two-component fuel mixtures of hydrogen, methane and propane, *Int. J. Hydrog. Energy* 34 (22) (2009) 9258–9265.
- [83] F. Dinkelacker, B. Manickam, S. Muppala, Modelling and simulation of lean premixed turbulent methane/hydrogen/air flames with an effective lewis number approach, *Combust. Flame* 158 (9) (2011) 1742–1749.
- 585 [84] N. Bouvet, F. Halter, C. Chauveau, Y. Yoon, On the effective lewis number formulations for lean hydrogen/hydrocarbon/air mixtures, *Int. J. Hydrog. Energy* 38 (14) (2013) 5949–5960.
- [85] C. Liu, S. Shy, C. Chiu, M. Peng, H. Chung, Hydrogen/carbon monoxide syngas burning rates measurements in high-pressure quiescent and turbulent environment, *Int. J. Hydrog. Energy* 36 (14) (2011) 8595–8603.
- 590 [86] C.-W. Zhou, Y. Li, U. Burke, C. Banyon, K. P. Somers, S. Ding, S. Khan, J. W. Hargis, T. Sikes, O. Mathieu, et al., An experimental and chemical kinetic modeling study of 1, 3-butadiene combustion: Ignition delay time and laminar flame speed measurements, *Combust. Flame* 197 (2018) 423–438.
- [87] P. Glarborg, J. A. Miller, B. Ruscic, S. J. Klippenstein, Modeling nitrogen chemistry in combustion, *Prog. Energy Combust. Sci* 67 (2018) 31–68.

- 595 [88] CSPTk - a software toolkit for the CSP and TSR analysis of kinetic models and the simplification and reduction of chemical kinetics mechanisms. The software can be obtained upon request to M.Valorani (mauro.valorani@uniroma1.it), Tech. rep., Sapienza University of Rome, Italy (2015).
- [89] C. Safta, H. N. Najm, O. Knio, TChem-a software toolkit for the analysis of complex kinetic models, Sandia Report, SAND2011-3282.
- 600 [90] X. Hui, D. Zheng, C. Zhang, X. Xue, C.-J. Sung, Effects of hydrogen peroxide addition on two-stage ignition characteristics of n-heptane/air mixtures, *Int. J. Hydrog. Energy* 44 (44) (2019) 24312–24320.
- [91] C. K. Law, *Combustion Physics*, Cambridge University Press, New York, 2006.
- [92] E.-A. Tingas, D. C. Kyritsis, D. A. Goussis, H<sub>2</sub>/air autoignition dynamics around the third explosion limit, *J. Energy Eng.* 145 (1) (2019) 04018074.
- 605 [93] A. Kéromnès, W. K. Metcalfe, K. A. Heufer, N. Donohoe, A. K. Das, C.-J. Sung, J. Herzler, C. Naumann, P. Griebel, O. Mathieu, et al., An experimental and detailed chemical kinetic modeling study of hydrogen and syngas mixture oxidation at elevated pressures, *Combust. Flame* 160 (6) (2013) 995–1011.